Noncoherent Short Packet Detection and Decoding for Scatter Radio Sensor Networking

Panos N. Alevizos, *Student Member, IEEE*, Aggelos Bletsas, *Senior Member, IEEE*, and George N. Karystinos, *Member, IEEE*

Abstract

Scatter radio, i.e., communication by means of reflection, has been recently proposed as a promising technology for low-power wireless sensor networks (WSN). Specifically, this work offers noncoherent receivers in scatter radio frequency-shift keying (FSK), for either channel-coded or uncoded scatter radio reception, in order to eliminate the need for training bits of coherent schemes (for channel estimation) at the packet preamble. Noncoherent symbol-by-symbol and sequence detectors based on hybrid composite hypothesis test (HCHT) and generalized likelihood-ratio test (GLRT), for the uncoded case and noncoherent decoders based on HCHT, for small block-length channel codes, are derived. Performance comparison under Rician, Rayleigh or no fading, taking into account fixed energy budget per packet is presented. It is shown that the performance gap between coherent and noncoherent reception depends on whether channel codes are employed, the fading conditions (e.g., Rayleigh vs Rician vs no fading), as well as the utilized coding interleaving depth; the choice of one coding scheme over the other depends on the wireless fading parameters and the design choice for extra diversity vs extra power gain. Finally, experimental outdoor results at 13 dBm transmission power corroborate the practicality of the proposed noncoherent detection and decoding techniques for scatter radio WSNs.

Index Terms

Backscatter sensor networks, noncoherent detection/decoding, generalized likelihood-ratio test, composite hypothesis test, frequency-shift keying, Rician fading.

Authors are with School of Electrical and Computer Engineering (ECE), Technical University of Crete, Chania 73100, Greece. (E-mail: palevizos@isc.tuc.gr, {aggelos, karystinos}@telecom.tuc.gr)

I. INTRODUCTION

Networking thousands of sensors in a given geographical area, sensing time-dependent environmental variables (e.g., soil humidity, soil moisture, temperature, solar irradiance) and gathering the sensed information at a central receiver, is a challenging task. Existing, commercial wireless sensor network (WSN) equipment involves Marconi radios, consisting of signal conditioning radio frequency (RF) components, such as amplifiers, mixers or filters, increasing complexity, monetary cost, and energy consumption per sensor node, even for low bitrate applications. On the other hand, scatter radio, i.e., communication by means of reflection, has been recently proposed as a promising enabling, low-power, and cost-effective solution for WSNs [1].

Scatter radio is principally encountered in radio frequency identification (RFID) systems, mainly utilized in supply chain monitoring and object tracking [2]. The basic ingredients of current scatter radio technology include the illuminating transmitter towards the tags, the reflecting tags, that may be passive (i.e., powered by the illuminating RF field) or semi-passive (i.e., power by an ambient source or an external battery) and the receiving reader of the backscattered (from the tags) signals. Typical scatter radio RFID systems are monostatic, i.e., illuminating transmitter and receiver belong to the same unit, a.k.a. *the reader*. RFID systems suffer from limited range, in the order of a few meters, due to a) limited RF harvesting efficiency and sensitivity in existing passive tags, b) monostatic design principles that jointly address two orthogonal aspects, i.e., illumination for communication and illumination for powering of all scatter radio tags, and c) high bitrate adopted by commercial tags, reducing the received energy per bit.

In an effort to increase communication range, work in [1] considered semi-passive tags, i.e., scatter radio tags with external power source; since scatter radio modulation only needs termination of the tag/sensor antenna at different loads, ultra-low power is required, available at a battery or an ambient source, such as solar, RF or their combination [3], enabling perpetual sensing [4] even at small levels of ambient power [5]. Specifically, work in [1] studied low bitrate symbol-by-symbol noncoherent reception of minimum-shift keying (MSK) for monostatic scatter radio; the frequency-shift keying (FSK) aspect allowed receiver-less tags and, in principle, no tag collision at the reader, since each tag was allocated a unique portion of the spectrum (frequency-division multiplexing by receiver-less tags). Subsequent work in [6] studied interference in monostatic scatter radio architectures from frequency reuse, when several monostatic readers serve a given geographic area. Work in [7], [8] studied fading and correlation of the two-way

(from illuminating antennas to tags and from tags back to the reader), backscatter radio channel, with emphasis on multi-antenna systems, while work in [9], [10] examined link budgets and gains in multi-antenna backscatter systems. Work in [11] studied multi-user detection techniques for single- and multiple-antenna tag collision recovery receivers, i.e., reception when two or more tags scatter back nonorthogonally, while work in [12] offered single-antenna detectors for two-collided scatter radio tags, exploiting the inherent memory of specific lines codes used in commercial RFID. Recent work in [13] offered the complete processing chain of coherent maximum-likelihood (ML) reception of Gen2 RFID tags, with commodity, monostatic software-defined radio (SDR) reader, also exploiting the inherent memory of specific line codes used in the RFID protocol.

Bistatic scatter radio, where the illuminating emitter is a distinct unit, located at a different location than the receiver of the signals reflected by the tag(s), was first experimentally demonstrated in [14]–[16], with tags employing scatter radio FSK or on-off keying (OOK) and SDR symbol-by-symbol noncoherent receiver; ranges one order of magnitude larger than conventional RFID were observed, also highlighting the additional difficulties due to the bistatic nature (e.g., carrier frequency offset between illuminating emitter and receiver) or the scatter radio nature (e.g., modulation at passband and different than conventional FSK radio signal model requiring modification of the reception algorithms). Work in [17] employed small block-length error-correction channel codes for inherently resource-constrained sensors/tags and experimentally demonstrated heuristic soft-decision metrics for noncoherent decoding with FSK and bistatic principles; communication range increase was shown, compared to the uncoded case. Subsequent work in [18] proposed coherent detection and decoding with small block-length cyclic channel codes for the bistatic scatter radio architecture with FSK modulation; the compound channel vector incorporated all wireless channel and microwave, tag-related parameters and was estimated with least-squares (LS), using a short training packet preamble (known at the receiver). Work in [19] offered noncoherent sequence detection of uncoded orthogonal signaling, also showing its relevance to commercial Gen2 RFID protocols. Proof-of-concept bistatic scatter radio WSN examples with analog FM principles can be found in [20] and [21], for environmental humidity and soil moisture, respectively, while work in [22] used bistatic scatter radio to convey the electric potential of several plants and each WSN terminal was powered by the plant itself, capitalizing upon the ultra-low power requirements of scatter radio. Work in [23] is also an example of bistatic scatter radio, where the system designers carefully utilized the *modulated* signals transmitted

from a DTV station, as the illuminating signal. Work in [24] and [25] demonstrated reception of bistatic scatter radio FSK with an *embedded* receiver for Bluetooth and UHF frequencies, respectively.

From a networking perspective, FSK also facilitates efficient multiple access schemes [26], [27]. Several ultra low-cost emitters, possibly powered through energy-harvesting techniques, can be stochastically placed in the field, illuminating multiple tags. Each tag, within a backscatter cell formed by any low-cost carrier emitter, can be associated with a unique part of the spectrum for the modulating scatter radio frequencies at each tag/sensor, facilitating frequency-division multiplexing (FDM). To mitigate interference among neighboring cells, carrier emitters can further utilize a time-division multiplexing (TDM) scheme. Relevant work has demonstrated such concrete FDM examples of collision-free, multiple access with receiver-less tags and analog (in [20]) or digital (in [27]) bistatic scatter radio principles.

This work is motivated by short packet communication (e.g., [28], [29] and references therein), given that scatter radio tags/sensors are constrained in terms of available energy, memory, computational power and relatively long channel codes may not be practically possible at the tag encoder. Moreover, low bitrate applications, as in environmental monitoring, in conjunction with the need for multi-user detection in software-defined platforms, favor the utilization of relatively smaller (than larger) packets, in order to reduce processing delay within practically meaningful limits. Thus, this work aims at noncoherent receivers for either coded or uncoded scatter radio reception, in order to eliminate the need for training bits at the packet preamble; the latter is necessary in coherent systems for channel estimation. The focus is on scatter radio FSK, in order to enable FDM and thus, zero collision networking of several (even receiver-less) tags/sensors. Specifically, this work:

- Proves that the square-law symbol-by-symbol detector for uncoded scatter radio FSK, first proposed in [16], is an instance of a—well known in estimation and detection theory—composite hypothesis test (CHT), and more specifically, of a hybrid CHT (HCHT).
- Proposes noncoherent symbol-by-symbol and sequence detectors for uncoded scatter radio FSK, based on generalized likelihood-ratio test (GLRT); the proposed noncoherent detectors are tailored to the scatter radio physical layer, with many parameters in principle unknown.
- Extends HCHT framework to the coded scatter radio setup and offers a noncoherent decoding rule, ideal for small packet and small block-length channel codes required with resource constrained scatter radio tags/sensors.

- Evaluates bit error rate (BER) performance of the proposed scatter radio receivers under Rician, Rayleigh or no fading, for *fixed* energy per packet. Interestingly, it is shown that for the uncoded case, noncoherent reception can outperform coherent reception under fixed energy per packet, taking also into account the energy spent at the preamble bits for channel estimation (in the coherent case). For the coded case, the performance gap between coherent and noncoherent reception depends on the fading conditions (e.g., Rayleigh vs Rician), as well as the utilized interleaving depth and possible diversity gain.
- Compares noncoherent performance of BCH or Reed-Muller codes of slightly different rates and Hamming distance, showing that the choice of one coding scheme over the other depends on the wireless fading parameters and the design choice for extra diversity vs extra power gain.
- Offers experimental outdoor measurements (with scatter radio testbed), corroborating the practicality of the proposed noncoherent detection and decoding techniques for scatter radio.

Compared to the conference version [30], this work additionally proposes GLRT symbol-by-symbol detector and GLRT sequence detector, includes full derivations and proofs, as well as comprehensive simulation and experimental (with scatter radio testbed) results.

The rest of the work is organized as follows: Section II presents the system model, showing how the bistatic signal model can also describe the monostatic, and describes the utilized modulation scheme. Section III designs noncoherent receivers for scatter radio FSK incorporated in the bistatic setup. Simulation and experimental results are offered in Section IV and V, respectively. Finally, conclusions are drawn in Section VI.

Notation: Symbols $(\cdot)^\top$, $(\cdot)^{\mathrm{H}}$, $(\cdot)^*$ will denote the transpose, Hermitian, and complex conjugate, respectively, of a vector or matrix. Real-part and imaginary-part operations are denoted by $\Re\{\cdot\}$ and $\Im\{\cdot\}$, respectively, The phase of a complex number z is denoted as $\angle z$. The distribution of a proper complex Gaussian $N \times 1$ vector $\mathbf{x}$ with mean $\boldsymbol{\mu}$ and covariance matrix $\boldsymbol{\Sigma}$ is denoted by $\mathcal{CN}(\boldsymbol{\mu}, \boldsymbol{\Sigma}) \stackrel{\triangle}{=} \frac{1}{\pi^N \det(\boldsymbol{\Sigma})} \mathrm{e}^{-(\mathbf{x}-\boldsymbol{\mu})^{\mathrm{H}} \boldsymbol{\Sigma}^{-1} (\mathbf{x}-\boldsymbol{\mu})}$. $\mathcal{U}[a, b)$ denotes the uniform distribution in $[a, b)$. The expectation operator associated with probability density function (PDF) $\mathrm{f}_{\mathbf{x}|\boldsymbol{\theta}}(\cdot|\cdot)$ of any function $\mathrm{g}(\mathbf{x}, \boldsymbol{\theta})$ is denoted as $\mathop{\mathbb{E}}_{\mathbf{x}|\boldsymbol{\theta}}[\mathrm{g}(\mathbf{x}, \boldsymbol{\theta})] \stackrel{\triangle}{=} \int_{\mathbf{x}} \mathrm{g}(\mathbf{x}, \boldsymbol{\theta}) \mathrm{f}_{\mathbf{x}|\boldsymbol{\theta}}(\mathbf{x}|\boldsymbol{\theta}) \mathrm{d}\mathbf{x}$.

II. Scatter Radio Signal Model

Bistatic scatter radio consists of a carrier emitter (CE), a RF tag, and a software-defined radio (SDR) reader (Fig. 1). Due to relatively small bitrate (in the order of kilo-bits per second), or

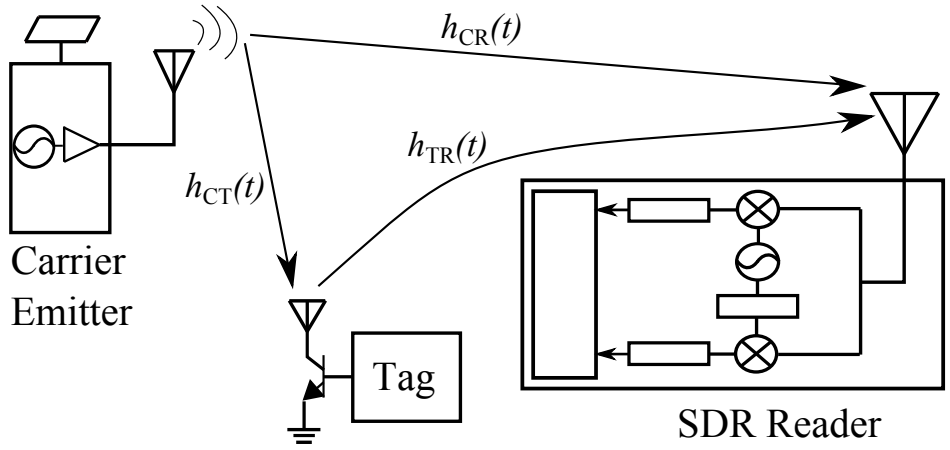

Fig. 1. Bistatic architecture: carrier emitter (CE) is located away from software-defined radio (SDR) reader; RF tag modulates and scatters the incident RF signal from CE towards the SDR reader.

equivalently large nominal bit period T, along with small delay spread, frequency non-selective (flat) fading channel [31] is assumed, with baseband complex channel response given by:

$$h_{\mathrm{m}}(t) = h_{\mathrm{m}} = a_{\mathrm{m}}\, \mathsf{e}^{-\mathrm{j}\phi_{\mathrm{m}}},\ \mathrm{m} \in \{\mathrm{CR}, \mathrm{CT}, \mathrm{TR}\}, \tag{1}$$

where $a_{\mathrm{CR}}, a_{\mathrm{CT}}, a_{\mathrm{TR}} \in \mathbb{R}_+$ denote the channel attenuation parameters of the corresponding links and $\phi_{\mathrm{CR}}, \phi_{\mathrm{CT}}, \phi_{\mathrm{TR}} \in [0, 2\pi)$ the respective phases. Due to the bistatic setup in Fig. 1, the distance between the antennas of different devices is several wavelengths apart and thus, the channel response parameters are considered statistically independent of each other; channel is assumed to change every T_{coh} seconds.

For outdoor WSN environments, typically there is a strong line-of-site (LOS) signal for each individual link and thus, channel parameters are assumed Rician random variables (RVs) [32], i.e., for $\mathrm{m} \in \{\mathrm{CR}, \mathrm{CT}, \mathrm{TR}\}$,

$$h_{\mathrm{m}} \sim \mathcal{CN}\left(\sqrt{\frac{\kappa_{\mathrm{m}}}{\kappa_{\mathrm{m}}+1}}\sigma_{\mathrm{m}}, \frac{\sigma_{\mathrm{m}}^2}{\kappa_{\mathrm{m}}+1}\right). \tag{2}$$

Parameter κ_{m} stands for the ratio between the power in the direct path and the power in the scattered paths of link $\mathrm{m} \in \{\mathrm{CR}, \mathrm{CT}, \mathrm{TR}\}$. For the special case of $\kappa_{\mathrm{m}} = 0$, Rayleigh fading is obtained, while for $\kappa_{\mathrm{m}} = \infty$, Gaussian channel is obtained with parameters a_{m} being deterministic, i.e., $a_{\mathrm{m}} = \sigma_{\mathrm{m}}$. Note that the channel power at link m is given by $\mathbb{E}\left[|h_{\mathrm{m}}|^2\right] = \sigma_{\mathrm{m}}^2$, i.e., it is independent of κ_{m}. For exposition purposes and without loss of generality, $\sigma_{\mathrm{m}}^2 = 1,\ \mathrm{m} \in \{\mathrm{CR}, \mathrm{CT}, \mathrm{TR}\}$, is assumed.

CE transmits a continuous carrier wave at carrier frequency $F_{\rm car}$ with complex baseband representation given by:

$$\mathsf{c}(t) = \sqrt{2P_{\rm C}}\ \mathsf{e}^{-\mathrm{j}(2\pi\Delta F t + \Delta\phi)}, \tag{3}$$

where $P_{\rm C}$ is the carrier transmitting power at passband, ΔF and $\Delta\phi$ model the carrier frequency and carrier phase offset between CE and SDR reader, respectively. $\Delta\phi$ is modeled as a uniform RV in $[0, 2\pi)$.

Tag is illuminated by the carrier wave $\mathsf{c}(t)$, attenuated and rotated due to the channel gain $a_{\rm CT}\,\mathsf{e}^{-\mathrm{j}\phi_{\rm CT}}$. The reflected waveform is further attenuated by a real parameter s, related to the tag's scattering efficiency (as well as potential RF harvesting ability), considered constant during packet transmission. For two distinct tag load values (and thus, binary modulation at the tag), the baseband scattered waveform can be written as [16]:

$$\mathsf{u}_i(t) = \mathsf{s}\left(\mathsf{v}_0 + \frac{\Gamma_0 - \Gamma_1}{2}\,\mathsf{b}_i(t)\right)\ a_{\rm CT}\,\mathsf{e}^{-\mathrm{j}\phi_{\rm CT}}\mathsf{c}(t),\ \ i \in \mathbb{B}, \tag{4}$$

where $\mathsf{b}_i(t)$ corresponds to the complex baseband waveform for bit $i \in \mathbb{B} \triangleq \{0, 1\}$. The term $\mathsf{v}_0 = \mathsf{A}_s - \frac{\Gamma_0+\Gamma_1}{2}$ is a DC constant that depends on the (load-independent) tag antenna structural mode A_s [6] and the (tag load-dependent) tag reflection coefficients Γ_0 and Γ_1. Scatter radio modulator at each tag/sensor does not include any type of signal conditioning units (e.g., amplifiers, filters or mixers); instead, each tag's antenna is connected to a load through a controllable switch and thus, there is no noise term in Eq. (4). The absence of signal conditioning at each tag offers low power consumption and is the main advantage of scatter radio.

For FSK modulation, waveform $\mathsf{b}_i(t)$ represents the fundamental frequency component of a 50% duty cycle square waveform[1] of period $1/F_i$ and random initial phase Φ_i:

$$\mathsf{b}_i(t) = \frac{4}{\pi}\,\mathsf{cos}(2\pi F_i t + \Phi_i)\ \Pi_T(t), \quad i \in \mathbb{B}, \tag{5}$$

where $\Pi_T(t)$ is the rectangular pulse of bit duration T, given by:

$$\Pi_T(t) \triangleq \begin{cases} 1, & 0 \le t < T, \\ 0, & \text{otherwise.} \end{cases} \tag{6}$$

[1]It can be shown that the fundamental frequency component holds $\approx 80\%$ of the total power of the 50% duty cycle square pulse [1].

$\Phi_i \sim \mathcal{U}[0, 2\pi)$ models the phase mismatch between tag and SDR reader (when bit $i \in \mathbb{B}$ is transmitted) and is assumed constant during packet transmission; furthermore, Φ_0 is assumed independent of Φ_1. $\mathbf{\Phi} \triangleq [\Phi_0 \ \Phi_1]^\top$ is also defined.

For time t within a single bit duration T, the received demodulated complex baseband signal at the SDR reader is given by the superposition of the CE sinusoid and the backscattered tag signal through channels $h_{\rm CR}$ and $h_{\rm TR}$, respectively:

$$\mathsf{y}(t) = a_{\rm CR}\, \mathsf{e}^{-\mathrm{j}\phi_{\rm CR}}\, \mathsf{c}(t) + a_{\rm TR}\, \mathsf{e}^{-\mathrm{j}\phi_{\rm TR}}\, \mathsf{u}_i(t) + \mathsf{n}(t), \tag{7}$$

where $\mathsf{n}(t)$ is circularly symmetric, complex, additive Gaussian noise process with power spectral density given by:

$$\mathsf{S}_{\rm n}(F) = \begin{cases} \frac{N_0}{2}, & |F| \leq W_{\rm SDR} \\ 0, & \text{otherwise,} \end{cases} \tag{8}$$

where $W_{\rm SDR}$ denotes the SDR receiver bandwidth.

The signal in Eq. (7) contains carrier frequency offset (CFO) ΔF, which can be directly estimated using periodogram-based techniques, and subsequently, compensated. CFO estimation depends on all terms of Eq. (7), including those where no tag information is modulated.[2] After CFO compensation, the DC terms of the signal in (7) can be eliminated, by estimation and removal of the received signal's time average [16]. After synchronization and CFO estimation, the DC-blocked received signal of Eq. (7) within a bit period T, is simplified to:

$$\widetilde{\mathsf{y}}(t) = \mu\, a\, \mathsf{e}^{-\mathrm{j}\phi}\, \mathsf{cos}\left(2\pi F_i t + \Phi_i\right) \Pi_T(t) + \mathsf{n}(t), \tag{9}$$

where the following abbreviations are utilized:

$$\phi \triangleq \phi_{\rm CT} + \phi_{\rm TR} + \Delta\phi + \underline{/\Gamma_0 - \Gamma_1}, \tag{10}$$

$$a \triangleq a_{\rm CT}\, a_{\rm TR}, \tag{11}$$

$$\mu \triangleq \sqrt{2P_{\rm C}}\, \frac{|\Gamma_0 - \Gamma_1|}{2}\, \frac{4}{\pi}\, \mathsf{s} = \sqrt{2P_{\rm C}}\, |\Gamma_0 - \Gamma_1|\, \frac{2}{\pi}\, \mathsf{s}. \tag{12}$$

The signal in (9) can be equivalently written as follows:

$$\widetilde{\mathsf{y}}(t) = \frac{\mu\, h}{2} \left(\mathsf{e}^{\mathrm{j}(2\pi F_i t + \Phi_i)} + \mathsf{e}^{-\mathrm{j}(2\pi F_i t + \Phi_i)}\right) \Pi_T(t) + \mathsf{n}(t), \tag{13}$$

[2]Therefore, tag-dependent parameters such as $\mathtt{A}_s$, typically overlooked in the literature, do play important role in the CFO estimation step [16].

with parameter $h \triangleq a\,\mathsf{e}^{-\mathsf{j}\phi}$ including some phase and wireless channel fading parameters.

Assuming $F_i \gg \frac{1}{T}$, $i \in \mathbb{B}$, the instantaneous received energy per bit is defined as follows:

$$\mathrm{E}(a) \triangleq \int_0^T \left|\mu\, a\, \mathsf{e}^{-\mathsf{j}\phi}\mathsf{cos}(2\pi F_i t + \Phi_i)\right|^2 \mathsf{d}t \approx \frac{T\mu^2 a^2}{2}, \tag{14}$$

where $\int_0^T \mathsf{cos}^2(2\pi F_i t + \Phi_i)\mathsf{d}t \approx \frac{T}{2}$ is exploited. The average received energy per bit and the average received SNR are defined as:

$$\mathtt{E} = \mathop{\mathbb{E}}_{a}[\mathrm{E}(a)] = \frac{T\mu^2}{2} = \frac{4\,T\,P_{\mathrm{C}}\,|\Gamma_0 - \Gamma_1|^2\,\mathtt{s}^2}{\pi^2}, \tag{15}$$

$$\mathtt{SNR} \triangleq \frac{\mathtt{E}}{\frac{N_0}{2}} = \frac{T\mu^2}{N_0} = \frac{8\,T\,P_{\mathrm{C}}\,|\Gamma_0 - \Gamma_1|^2\,\mathtt{s}^2}{N_0\,\pi^2}. \tag{16}$$

From the received signal in (13) it can be immediately observed that for each bit $i \in \mathbb{B}$, two exponential frequencies $\pm F_i$ exist and not one; thus, a classic FSK demodulator for conventional (Marconi) radio loses half of the signal and results in a 3-dB BER performance loss for bistatic FSK [16]. It can be shown that for $|F_1 - F_0| = \frac{k}{T},\ k \in \mathbb{N}$, along with $F_i \gg \frac{1}{T}$, $i \in \mathbb{B}$ (that implies that $F_i + F_0 \gg \frac{1}{T}$ or $F_i + F_1 \gg \frac{1}{T}$), the set $\left\{\frac{1}{\sqrt{T}}\mathsf{e}^{\pm\mathsf{j}2\pi F_i t}\Pi_T(t)\right\}_{i\in\mathbb{B}}$ constitutes a 4-dimensional orthonormal basis, that can be used for expansion of the received signal in (13). According to [18, Theorem 1], for $F_i + \frac{20}{T} \ll W_{\mathrm{SDR}}$, the baseband equivalent signal over a bit duration T is given by the following 4-dimensional complex vector:

$$\mathbf{r} = \begin{bmatrix} r_0^+ \\ r_0^- \\ r_1^+ \\ r_1^- \end{bmatrix} = h\sqrt{\frac{\mathtt{E}}{2}} \begin{bmatrix} \mathsf{e}^{+\mathsf{j}\Phi_0} \\ \mathsf{e}^{-\mathsf{j}\Phi_0} \\ \mathsf{e}^{+\mathsf{j}\Phi_1} \\ \mathsf{e}^{-\mathsf{j}\Phi_1} \end{bmatrix} \odot \mathbf{s}_i + \begin{bmatrix} n_0^+ \\ n_0^- \\ n_1^+ \\ n_1^- \end{bmatrix}, \tag{17}$$

where vector $\mathbf{s}_i = [(1-i)\ \ (1-i)\ \ i\ \ i]^\top$ corresponds to bit $i \in \mathbb{B}$. Symbol $\odot$ denotes the component-wise (Hadamard) product and 4-dimensional complex, circularly symmetric Gaussian noise vector is distributed according to:

$$[n_0^+\ \ n_0^-\ \ n_1^+\ \ n_1^-]^\top \sim \mathcal{CN}\left(\mathbf{0}_4, \frac{N_0}{2}\mathbf{I}_4\right). \tag{18}$$

It is noted that the system model above has been verified experimentally [14]–[16], [20], [33], [34]. It is also noted that it is general enough to describe monostatic scatter radio (where illuminating carrier emitter and receiver belong to the same reader unit) as a special case, with h_{CR} (and appropriate $\kappa_{\mathrm{CR}}, \sigma_{\mathrm{CR}}$) modeling the leakage from the transmit to the receive RF chain of the reader.

III. Noncoherent Scatter Radio Detection and Decoding

A. Uncoded Symbol-By-Symbol Detection

The bit error rate (BER)-optimal maximum-likelihood (ML) rule with noncoherent symbol-by-symbol processing is given by:

$$\mathsf{f}_{\mathbf{r}|i}(\mathbf{r}|0) \underset{i=1}{\overset{i=0}{\gtrless}} \mathsf{f}_{\mathbf{r}|i}(\mathbf{r}|1) \Longleftrightarrow \tag{19}$$

$$\mathop{\mathbb{E}}_{h,\boldsymbol{\Phi}}\left[\mathsf{f}_{\mathbf{r}|i,h,\Phi_0}(\mathbf{r}|0,h,\Phi_0)\right] \underset{i=1}{\overset{i=0}{\gtrless}} \mathop{\mathbb{E}}_{h,\boldsymbol{\Phi}}\left[\mathsf{f}_{\mathbf{r}|i,h,\Phi_1}(\mathbf{r}|1,h,\Phi_1)\right].$$

Note that due to Eqs. (17) and (18),

$$\mathsf{f}_{\mathbf{r}|i,h,\boldsymbol{\Phi}}(\mathbf{r}|i,h,\boldsymbol{\Phi}) \equiv \mathcal{CN}\left(h\,\mathbf{x}_i(\boldsymbol{\Phi}), \frac{N_0}{2}\mathbf{I}_4\right), \tag{20}$$

with $\mathbf{x}_i(\boldsymbol{\Phi}) = \sqrt{\frac{\mathsf{E}}{2}}\left[\mathsf{e}^{+\mathsf{j}\Phi_0}, \mathsf{e}^{-\mathsf{j}\Phi_0}, \mathsf{e}^{+\mathsf{j}\Phi_1}, \mathsf{e}^{-\mathsf{j}\Phi_1}\right]^\top \odot \mathbf{s}_i$. For the bistatic scatter radio signal model, the ML rule does not admit closed form expression for Rician parameters $\kappa_{\mathrm{CT}}, \kappa_{\mathrm{TR}} \in [0, +\infty)$, and thus, alternative detection rules must be designed.

1) Noncoherent Hybrid Composite Hypothesis-Testing (NC-HCHT) Symbol-By-Symbol FSK Detection: The NC-HCHT symbol-by-symbol detection rule treats the unknowns Φ_0 and Φ_1 as random, while h is viewed as a nonrandom parameter; NC-HCHT detection is given by:

$$\arg\max_{i\in\mathbb{B}}\left\{\mathop{\mathbb{E}}_{\boldsymbol{\Phi}}\left[\max_{h\in\mathbb{C}} \mathsf{ln}\left[\mathsf{f}_{\mathbf{r}|i,h,\boldsymbol{\Phi}}(\mathbf{r}|i,h,\boldsymbol{\Phi})\right]\right]\right\}. \tag{21}$$

Lemma 1. The noncoherent detector of Eq. (21) is channel-agnostic and is equivalent to:

$$|r_0^+|^2 + |r_0^-|^2 \underset{i=1}{\overset{i=0}{\gtrless}} |r_1^+|^2 + |r_1^-|^2, \tag{22}$$

i.e., the detector in (21) is the square-law detector.

Proof. For hypothesis $i = 0$, $\mathbf{x}_0(\boldsymbol{\Phi})$ depends solely on Φ_0, i.e., $\mathbf{x}_0(\Phi_0)$, and the innermost maximization in (21) eliminates parameter h as follows:

$$\begin{aligned}&\arg\max_{h\in\mathbb{C}} \mathsf{ln}\left[\mathsf{f}_{\mathbf{r}|i,h,\Phi_0}(\mathbf{r}|0,h,\Phi_0)\right]\\ &= \arg\min_{h\in\mathbb{C}} \|\mathbf{r} - h\mathbf{x}_0(\Phi_0)\|_2^2 \Longrightarrow h_{\mathrm{opt}} = \frac{\left(\mathbf{x}_0(\Phi_0)\right)^{\mathrm{H}}\mathbf{r}}{\|\mathbf{x}_0(\Phi_0)\|_2^2}.\end{aligned} \tag{23}$$

Hence,

$$\begin{aligned}
&\max_{h\in\mathbb{C}} \ln\left[\mathsf{f}_{\mathbf{r}|i,h,\Phi_0}(\mathbf{r}|0,h,\Phi_0)\right] = \ln\left[\mathsf{f}_{\mathbf{r}|i,h,\Phi_0}(\mathbf{r}|0,h_{\rm opt},\Phi_0)\right] \\
&= 4\ln\left(\frac{2}{\pi N_0}\right) - \frac{1}{N_0}\left(2||\mathbf{r}||_2^2 - \left|(r_0^+)^*\mathsf{e}^{\mathsf{j}\Phi_0} + (r_0^-)^*\mathsf{e}^{-\mathsf{j}\Phi_0}\right|^2\right) \\
&= 4\ln\left(\frac{2}{\pi N_0}\right) - \frac{2}{N_0}||\mathbf{r}||_2^2 \\
&\quad + \frac{1}{N_0}\left(|r_0^+|^2 + |r_0^-|^2\right) + \frac{2}{N_0}\Re\left\{(r_0^+)^*(r_0^-)\mathsf{e}^{2\mathsf{j}\Phi_0}\right\}. \qquad (24)
\end{aligned}$$

Only the last term in (24) depends on Φ_0, and thus, applying expectation with respect to $\mathbf{\Phi}$ in the last term in (24) offers

$$\mathop{\mathbb{E}}_{\mathbf{\Phi}}\left[\Re\left\{(r_0^+)^*(r_0^-)\mathsf{e}^{2\mathsf{j}\Phi_0}\right\}\right] = \mathop{\mathbb{E}}_{\Phi_0}\left[\Re\left\{(r_0^+)^*(r_0^-)\mathsf{e}^{2\mathsf{j}\Phi_0}\right\}\right] = 0, \qquad (25)$$

where Eq. (25) stems from the fact that $\Phi_0 \sim \mathcal{U}[0, 2\pi)$. Therefore, applying expectation with respect to $\mathbf{\Phi}$ in (24) eliminates the last term. The same reasoning can be applied for hypothesis $i = 1$, since $\Phi_1 \sim \mathcal{U}[0, 2\pi)$. Thus, the detection rule of Eq. (22) is obtained. □

Interestingly, the above square-law detector has been also proposed in [16] as a heuristic noncoherent detection rule.

Proposition 1. For the special case of $\kappa_{\rm CT} = \kappa_{\rm TR} = 0$ (Rayleigh fading), detector in (22) offers BER given by:

$$\Pr(e) = \frac{\mathsf{e}^{\frac{2}{\mathtt{SNR}}}\left(5\mathtt{SNR}+2\right)\mathsf{E}_1\left(\frac{2}{\mathtt{SNR}}\right) - \mathtt{SNR}}{4\mathtt{SNR}^2}, \qquad (26)$$

where $\mathsf{E}_1(x) = \int_x^\infty \frac{\mathsf{e}^{-t}}{t}\mathsf{d}t$ for $x > 0$ [35, p. 150].

Proof. In Appendix A. □

2) Noncoherent Generalized Likelihood-Ratio Test (NC-GLRT) Symbol-By-Symbol FSK Detection: The NC-GLRT symbol-by-symbol detection rule treats the unknowns Φ_0, Φ_1 and h as nonrandom parameters and is expressed as follows:

$$\arg\max_{i\in\mathbb{B}}\left\{\max_{\mathbf{\Phi}\in[0,2\pi)^2}\max_{h\in\mathbb{C}} \ln\left[\mathsf{f}_{\mathbf{r}|i,h,\mathbf{\Phi}}(\mathbf{r}|i,h,\mathbf{\Phi})\right]\right\}. \qquad (27)$$

Theorem 1. The detector of Eq. (27) is channel-agnostic and is equivalent to:

$$|r_0^+| + |r_0^-| \underset{i=1}{\overset{i=0}{\gtrless}} |r_1^+| + |r_1^-|. \qquad (28)$$

Proof. The proof relies on fact that for any complex number α,

$$|\alpha| = \max_{v\in\mathbb{C}:|v|=1} \Re\{\alpha v^*\} = \max_{\varphi\in[0,2\pi)} \Re\{\alpha \mathsf{e}^{-\mathsf{j}\varphi}\}. \tag{29}$$

Using Lemma 1, for $i = 0$, the innermost maximization in (27) is simplified to Eq. (24), depending solely on Φ_0. Hence, applying maximization with respect to $\mathbf{\Phi} \in [0, 2\pi)^2$ in (24) affects only the last term; in view of (29), the following holds:

$$\max_{\Phi_1\in[0,2\pi)} \max_{\Phi_0\in[0,2\pi)} \Re\left\{(r_0^+)^*(r_0^-)\mathsf{e}^{2\mathsf{j}\Phi_0}\right\} = |r_0^+||r_0^-|, \tag{30}$$

where the fact that $\Re\left\{(r_0^+)^*(r_0^-)\mathsf{e}^{2\mathsf{j}\Phi_0}\right\}$ is a periodic function of Φ_0 with period π was considered. Thus,

$$\begin{aligned}&\max_{\mathbf{\Phi}\in[0,2\pi)^2} \max_{h\in\mathbb{C}} \mathsf{ln}\left[\mathsf{f}_{\mathbf{r}|i,h,\Phi_0}(\mathbf{r}|0,h,\Phi_0)\right]\\ &= 4\mathsf{ln}\left(\frac{2}{\pi N_0}\right) - \frac{2}{N_0}\|\mathbf{r}\|_2^2 + \frac{1}{N_0}\left(|r_0^+| + |r_0^-|\right)^2.\end{aligned} \tag{31}$$

Working similarly for $i = 1$, the result in (28) follows. □

B. Uncoded Sequence Detection

It is well understood that for bit period T smaller than channel coherence time T_{coh}, noncoherent symbol-by-symbol detection is not BER-optimal in flat fading and instead, noncoherent *sequence* detection must be employed (e.g., [36] and references therein). For static (immobile) scatter radio sensor networks, the above scenario of $T_{\mathrm{coh}} \gg T$ is possible. However, classic noncoherent sequence detection based on exhaustive search may be prohibitive, due to its exponential (in the sequence length) complexity. In this section, recent results in noncoherent sequence detection with log-linear complexity for orthogonal modulations [36] are exploited, to develop a relevant receiver for uncoded scatter radio sequence FSK, *noncoherently*, based on GLRT principles, denoted as NC-GLRT.

Let $T_{\mathrm{coh}} = N_{\mathrm{coh}}T$, where N_{coh} denotes the number of symbols affected by the same channel coefficient and let $N_{\mathrm{coh}} \in \mathbb{N}$, for simplicity. Transmission of a bit sequence consisting of N_{s} information bits is considered, $\mathbf{i} = [i_1\ i_2\ \ldots\ i_{N_{\mathrm{s}}}]^\top \in \mathbb{B}^{N_{\mathrm{s}}}$, where $N_{\mathrm{s}} \leq N_{\mathrm{coh}}$ and $N_{\mathrm{s}}T$ not larger than packet duration. The associated received sequence, over a duration of N_{s} bits consists of

the concatenation of N_{s} received vectors $\mathbf{r}_1, \mathbf{r}_2, \ldots, \mathbf{r}_{N_{\mathrm{s}}}$; each of them can be further expanded as in (17):

$$\mathbf{r}_{1:N_{\mathrm{s}}} = \begin{bmatrix} \mathbf{r}_1 \\ \mathbf{r}_2 \\ \vdots \\ \mathbf{r}_{N_{\mathrm{s}}} \end{bmatrix} = h \begin{bmatrix} \mathbf{x}_{i_1}(\mathbf{\Phi}) \\ \mathbf{x}_{i_2}(\mathbf{\Phi}) \\ \vdots \\ \mathbf{x}_{i_{N_{\mathrm{s}}}}(\mathbf{\Phi}) \end{bmatrix} + \begin{bmatrix} \mathbf{n}_1 \\ \mathbf{n}_2 \\ \vdots \\ \mathbf{n}_{N_{\mathrm{s}}} \end{bmatrix}, \tag{32}$$

where $\mathbf{r}_n = \begin{bmatrix} r_0^+(n) & r_0^-(n) & r_1^+(n) & r_1^-(n) \end{bmatrix}^\top$ stands for the 4-dimensional received vector for the nth time instant and

$$\mathbf{x}_{i_n}(\mathbf{\Phi}) \triangleq \sqrt{\frac{\mathsf{E}}{2}} \begin{bmatrix} \mathsf{e}^{\mathsf{j}\Phi_0} & \mathsf{e}^{-\mathsf{j}\Phi_0} & \mathsf{e}^{\mathsf{j}\Phi_1} & \mathsf{e}^{-\mathsf{j}\Phi_1} \end{bmatrix}^\top \odot \mathbf{s}_{i_n}, \tag{33}$$

with $\mathbf{s}_{i_n} = [1 - i_n \;\; 1 - i_n \;\; i_n \;\; i_n]^\top$, $i_n \in \mathbb{B}$, $n = 1, 2, ..., N_{\mathrm{s}}$. Using the same reasoning with (18), the noise statistics in Eq. (32) are $\begin{bmatrix} \mathbf{n}_1^\top & \mathbf{n}_2^\top & \ldots & \mathbf{n}_{N_{\mathrm{s}}}^\top \end{bmatrix}^\top \sim \mathcal{CN}\left(\mathbf{0}_{4N_{\mathrm{s}}}, \frac{N_0}{2}\mathbf{I}_{4N_{\mathrm{s}}}\right)$. Additionally, vector $\mathbf{x_i}(\mathbf{\Phi}) \triangleq \begin{bmatrix} \mathbf{x}_{i_1}^\top(\mathbf{\Phi}) & \mathbf{x}_{i_2}^\top(\mathbf{\Phi}) & \ldots & \mathbf{x}_{i_{N_{\mathrm{s}}}}^\top(\mathbf{\Phi}) \end{bmatrix}^\top$ is also defined. From (32) and the noise statistics above, the following is obtained,

$$\mathsf{f}_{\mathbf{r}_{1:N_{\mathrm{s}}}|\mathbf{i},h,\mathbf{\Phi}}\left(\mathbf{r}_{1:N_{\mathrm{s}}}|\mathbf{i}, h, \mathbf{\Phi}\right) \equiv \mathcal{CN}\left(h\,\mathbf{x_i}(\mathbf{\Phi}), \frac{N_0}{2}\mathbf{I}_{4N_{\mathrm{s}}}\right), \tag{34}$$

implying that $\mathbf{r}_1, \mathbf{r}_2, .., \mathbf{r}_{N_{\mathrm{s}}}$ are conditionally independent of each other given parameters h, $\mathbf{\Phi}$, and any transmitted sequence $\mathbf{i}$. As in Section III-A2, NC-GLRT detection metric over the sequence $\mathbf{i}$ is expressed as follows:

$$\begin{aligned} &\max_{\mathbf{i}\in\mathbb{B}^{N_{\mathrm{s}}}} \max_{\mathbf{\Phi}\in[0,2\pi)^2} \max_{h\in\mathbb{C}} \mathsf{ln}\left[\mathsf{f}_{\mathbf{r}_{1:N_{\mathrm{s}}}|\mathbf{i},h,\mathbf{\Phi}}\left(\mathbf{r}_{1:N_{\mathrm{s}}}|\mathbf{i}, h, \mathbf{\Phi}\right)\right] \\ &= \max_{\mathbf{\Phi}\in[0,2\pi)^2} \max_{\mathbf{i}\in\mathbb{B}^{N_{\mathrm{s}}}} \max_{h\in\mathbb{C}} \mathsf{ln}\left[\mathsf{f}_{\mathbf{r}_{1:N_{\mathrm{s}}}|\mathbf{i},h,\mathbf{\Phi}}\left(\mathbf{r}_{1:N_{\mathrm{s}}}|\mathbf{i}, h, \mathbf{\Phi}\right)\right]. \end{aligned} \tag{35}$$

For fixed $\mathbf{\Phi} \in [0, 2\pi)^2$ in (35), in accordance with the derivation of (24) in Lemma 1,

$$\begin{aligned} &\arg\max_{\mathbf{i}\in\mathbb{B}^{N_{\mathrm{s}}}} \max_{h\in\mathbb{C}} \mathsf{ln}\left[\mathsf{f}_{\mathbf{r}_{1:N_{\mathrm{s}}}|\mathbf{i},h,\mathbf{\Phi}}\left(\mathbf{r}_{1:N_{\mathrm{s}}}|\mathbf{i}, h, \mathbf{\Phi}\right)\right] \\ &= \arg\max_{\mathbf{i}\in\mathbb{B}^{N_{\mathrm{s}}}} \left|\left(\mathbf{r}_{1:N_{\mathrm{s}}}\right)^{\mathrm{H}} \mathbf{x_i}(\mathbf{\Phi})\right|, \end{aligned} \tag{36}$$

where Eq. (36) was obtained by plugging in the optimal h, $h_{\mathrm{opt}} = \frac{(\mathbf{x_i}(\mathbf{\Phi}))^{\mathrm{H}}\mathbf{r}_{1:N_{\mathrm{s}}}}{||\mathbf{x_i}(\mathbf{\Phi})||_2^2}$ and dropping out terms that do not affect the optimization problem. Thus, using Eq. (36) in conjunction with the

identity in (29) for $\alpha = \left(\mathbf{r}_{1:N_\mathrm{s}}\right)^{\mathrm{H}} \mathbf{x}_{\mathbf{i}}(\mathbf{\Phi})$, the NC-GLRT optimization problem in Eq. (35) can be equivalently expressed as follows:

$$\max_{\mathbf{\Phi}\in[0,2\pi)^2} \max_{\mathbf{i}\in\mathbb{B}^{N_\mathrm{s}}} \left| \left(\mathbf{r}_{1:N}\right)^{\mathrm{H}} \mathbf{x}_{\mathbf{i}}(\mathbf{\Phi}) \right| \tag{37}$$

$$= \max_{\mathbf{\Phi}\in[0,2\pi)^2} \max_{\mathbf{i}\in\mathbb{B}^{N_\mathrm{s}}} \max_{\varphi\in[0,2\pi)} \Re\left\{ \left(\left(\mathbf{r}_{1:N}\right)^{\mathrm{H}} \mathbf{x}_{\mathbf{i}}(\mathbf{\Phi}) \right) \mathsf{e}^{-\mathrm{j}\varphi} \right\}$$

$$= \max_{\mathbf{\Phi}\in[0,2\pi)^2} \max_{\varphi\in[0,2\pi)} \max_{\mathbf{i}\in\mathbb{B}^{N_\mathrm{s}}} \sum_{n=1}^{N_\mathrm{s}} \Re\left\{ (\mathbf{r}_n)^{\mathrm{H}} \mathbf{x}_{i_n}(\mathbf{\Phi}) \mathsf{e}^{-\mathrm{j}\varphi} \right\}. \tag{38}$$

For fixed $\mathbf{\Phi} \in [0, 2\pi)^2$ and $\varphi \in [0, 2\pi)$, the innermost maximization in Eq. (38) splits into independent maximizations for any $n = 1, 2, \ldots, N_\mathrm{s}$, as

$$\widehat{i_n}(\mathbf{\Phi}, \varphi) = \arg\max_{i\in\mathbb{B}} \Re\left\{ (\mathbf{r}_n)^{\mathrm{H}} \mathbf{x}_i(\mathbf{\Phi}) \mathsf{e}^{-\mathrm{j}\varphi} \right\}$$

$$\Longleftrightarrow \Re\left\{ (\mathbf{r}_n)^{\mathrm{H}} \left(\mathbf{x}_0(\Phi_0) - \mathbf{x}_1(\Phi_1)\right) \mathsf{e}^{-\mathrm{j}\varphi} \right\} \underset{\widehat{i_n}(\mathbf{\Phi},\varphi)=1}{\overset{\widehat{i_n}(\mathbf{\Phi},\varphi)=0}{\gtrless}} 0$$

$$\Longleftrightarrow \cos\Big(\underline{\angle (\mathbf{r}_n)^{\mathrm{H}} \left(\mathbf{x}_0(\Phi_0) - \mathbf{x}_1(\Phi_1)\right)} - \varphi \Big) \underset{\widehat{i_n}(\mathbf{\Phi},\varphi)=1}{\overset{\widehat{i_n}(\mathbf{\Phi},\varphi)=0}{\gtrless}} 0. \tag{39}$$

For fixed $\mathbf{\Phi} \in [0, 2\pi)^2$, as φ scans $[0, 2\pi)$, the decision $\widehat{i_n}(\mathbf{\Phi}, \varphi)$ changes, according to Eq. (39), only when:

$$\cos\Big(\underline{\angle (\mathbf{r}_n)^{\mathrm{H}} \left(\mathbf{x}_0(\Phi_0) - \mathbf{x}_1(\Phi_1)\right)} - \varphi \Big) = 0 \tag{40}$$

$$\Longleftrightarrow \varphi = \underbrace{\pm\frac{\pi}{2} + \underline{\angle (\mathbf{r}_n)^{\mathrm{H}} \left(\mathbf{x}_0(\Phi_0) - \mathbf{x}_1(\Phi_1)\right)} \pmod{2\pi}}_{\varphi_n^{(1)}, \varphi_n^{(2)}}.$$

Hence, for fixed $\mathbf{\Phi} \in [0, 2\pi)^2$ the decision sequence $\widehat{\mathbf{i}}(\mathbf{\Phi}, \varphi) = \left[\widehat{i_1}(\mathbf{\Phi}, \varphi) \ \widehat{i_2}(\mathbf{\Phi}, \varphi) \ \ldots \ \widehat{i_{N_\mathrm{s}}}(\mathbf{\Phi}, \varphi) \right]^\top$ changes only at

$$\varphi_1^{(1)}, \varphi_1^{(2)}, \varphi_2^{(1)}, \varphi_2^{(2)}, \ldots, \varphi_{N_\mathrm{s}}^{(1)}, \varphi_{N_\mathrm{s}}^{(2)}, \tag{41}$$

where $0 < \varphi_n^{(l)} < 2\pi$, for any $n = 1, 2, \ldots, N_\mathrm{s}$, $l \in \{1, 2\}$. Since the $2N_\mathrm{s}$ points are distinct, only an element of decision $\widehat{\mathbf{i}}(\mathbf{\Phi}, \varphi)$ changes at each such point [36]. By sorting the above points in ascending order, i.e.,

$$(\theta_1, \theta_2, \ldots, \theta_{2N_\mathrm{s}}) = \mathsf{sort}\Big(\varphi_1^{(1)}, \varphi_1^{(2)}, \varphi_2^{(1)}, \ldots, \varphi_{N_\mathrm{s}}^{(1)}, \varphi_{N_\mathrm{s}}^{(2)} \Big), \tag{42}$$

then the decision $\widehat{\mathbf{i}}(\mathbf{\Phi}, \varphi)$ remains constant in each one of the $2N_\mathrm{s}$ intervals:

$$\mathcal{J}_0 = [\theta_0, \theta_1), \ \mathcal{J}_1 = [\theta_1, \theta_2), \ldots, \ \mathcal{J}_{2N_\mathrm{s}-1} = [\theta_{2N_\mathrm{s}-1}, \theta_{2N_\mathrm{s}}), \tag{43}$$

with $\theta_0 = 0$. It is noted that the interval $[\theta_{2N_\mathrm{s}}, 2\pi)$ is ignored because it corresponds to the same sequence $\widehat{\mathbf{i}}(\mathbf{\Phi}, \varphi)$ with $\mathcal{J}_0$. Thus, for fixed $\mathbf{\Phi} \in [0, 2\pi)^2$, our objective is the identification of the $2N_\mathrm{s}$ sequences $\widehat{\mathbf{i}}(\mathbf{\Phi}, 0), \widehat{\mathbf{i}}(\mathbf{\Phi}, \theta_1), \ldots, \widehat{\mathbf{i}}(\mathbf{\Phi}, \theta_{2N_\mathrm{s}-1})$, one of which offers the largest metric of interest, i.e., Eq. (37). The procedure of finding the best sequence $\widehat{\mathbf{i}}^\star(\mathbf{\Phi}) \triangleq \widehat{\mathbf{i}}(\mathbf{\Phi}, \theta_{\mathrm{opt}})$ is given in Algorithm 1. For given $\mathbf{\Phi} \in [0, 2\pi)^2$, the algorithm offers the GLRT-optimal sequence following the same principles with sequence detection algorithm developed in [36], with complexity $\mathcal{O}(N_\mathrm{s} \mathsf{log} N_\mathrm{s})$.

After obtaining the sequence $\widehat{\mathbf{i}}^\star(\mathbf{\Phi})$ the optimal phase pair $\mathbf{\Phi}^\star$ is given by:

$$\mathbf{\Phi}^\star = \arg \max_{\mathbf{\Phi} \in [0, 2\pi)^2} \left| \left(\mathbf{r}_{1:N_\mathrm{s}}\right)^{\mathrm{H}} \mathbf{x}_{\widehat{\mathbf{i}}^\star(\mathbf{\Phi})}(\mathbf{\Phi}) \right|. \tag{44}$$

and satisfies the following:

$$\widehat{\mathbf{i}}^\star(\mathbf{\Phi}^\star) = \widehat{\mathbf{i}}_{\mathrm{GLRT}}. \tag{45}$$

There is no readily available closed-form solution of problem in Eq. (44), thus, the following approach is instead utilized.

As a practical intuitive alternative, a natural number $M \in \mathbb{N}$ is chosen and the following set is formed:

$$\mathcal{W}_M \triangleq \left\{ 0, \frac{2\pi}{M}, \frac{4\pi}{M}, \ldots, \frac{(M-1)2\pi}{M} \right\} \subset [0, 2\pi), \tag{46}$$

and instead of solving the problem in Eq. (44), the following optimization problem is formed:

$$\widetilde{\mathbf{\Phi}}^\star_M = \arg \max_{\mathbf{\Phi} \in (\mathcal{W}_M)^2} \left| \left(\mathbf{r}_{1:N}\right)^{\mathrm{H}} \mathbf{x}_{\widehat{\mathbf{i}}^\star(\mathbf{\Phi})}(\mathbf{\Phi}) \right|. \tag{47}$$

The optimal phase pair for the above problem, $\widetilde{\mathbf{\Phi}}^\star_M$, offers sequence decision $\widehat{\mathbf{i}}^\star\left(\widetilde{\mathbf{\Phi}}^\star_M\right)$, which converges to $\widehat{\mathbf{i}}_{\mathrm{GLRT}}$ as $M \longrightarrow \infty$. Appropriate finite values of M are examined numerically. The above procedure is illustrated in Algorithm 2 and enjoys complexity of $\mathcal{O}(M^2 N_\mathrm{s} \mathsf{log} N_\mathrm{s})$, since there are M^2 Φ-pairs and for each pair, a sequence is found with $\mathcal{O}(N_\mathrm{s} \mathsf{log} N_\mathrm{s})$, while the quality metric for each sequence (in order to find the "best") is computed with linear in N_s complexity.

C. Noncoherent Coded Reception/Decoding

The idea of error-correction (channel) coding in bistatic scatter radio sensor networks is challenging; scatter radio tags are inherently resource-constrained, and thus, encoding at each tag/sensor must be computationally affordable. Additionally, the SDR reader must also employ low-complexity detection and decoding, in order to concurrently serve as many as possible frequency-modulated tags in a given spectrum band.

Algorithm 1 GLRT_Sequence_Detection_Given_$\mathbf{\Phi}$

Input: $\mathbf{r}_{1:N_\mathrm{s}} = \left[\mathbf{r}_1^\top \ \mathbf{r}_2^\top \ \ldots \ \mathbf{r}_{N_\mathrm{s}}^\top\right]^\top, \mathbf{\Phi} = [\Phi_0 \ \Phi_1]^\top$

for $n = 1 : N_\mathrm{s}$ **do**
  $\varphi_n^{(1)} := +\frac{\pi}{2} + \underline{\angle (\mathbf{r}_n)^\mathrm{H} \left(\mathbf{x}_0(\Phi_0) - \mathbf{x}_1(\Phi_1)\right)} \pmod{2\pi}$
  $\varphi_n^{(2)} := -\frac{\pi}{2} + \underline{\angle (\mathbf{r}_n)^\mathrm{H} \left(\mathbf{x}_0(\Phi_0) - \mathbf{x}_1(\Phi_1)\right)} \pmod{2\pi}$
end for
$(\theta_1, \theta_2, \ldots, \theta_{2N}) := \mathsf{sort}\left(\varphi_1^{(1)}, \varphi_1^{(2)}, \varphi_2^{(1)}, \ldots, \varphi_N^{(1)}, \varphi_N^{(2)}\right)$
for $n = 1 : N_\mathrm{s}$ **do**
  $\widehat{i_n}(\mathbf{\Phi}, 0) \equiv \gamma_n := \arg \max_{i \in \{0,1\}} \Re\left\{(\mathbf{r}_n)^\mathrm{H} \mathbf{x}_i(\mathbf{\Phi})\right\}$
end for
$m_\mathrm{cur} := \sum_{n=1}^{N_\mathrm{s}} (\mathbf{r}_n)^\mathrm{H} \mathbf{x}_{\gamma_n}(\mathbf{\Phi})$
$v_\mathrm{best} := |m_\mathrm{cur}|$
$\widehat{\mathbf{i}^\star}(\mathbf{\Phi}) := [\gamma_1 \ \gamma_2 \ \ldots \ \gamma_{N_\mathrm{s}}]^\top$
for $j = 1 : 2N_\mathrm{s} - 1$ **do**
  let n be the index: $\theta_j = \varphi_n^{(l)}$ for some $l \in \{1, 2\}$
  $\gamma := \widehat{i_n}(\mathbf{\Phi}, \theta_{j-1})$
  $\zeta := 1 - \gamma$
  $m_\mathrm{cur} := m_\mathrm{cur} + (\mathbf{r}_n)^\mathrm{H} \left(\mathbf{x}_\zeta(\mathbf{\Phi}) - \mathbf{x}_\gamma(\mathbf{\Phi})\right)$
  $\widehat{i_n}(\mathbf{\Phi}, \theta_j) := \zeta$
  $v_\mathrm{cur} := |m_\mathrm{cur}|$
  if $v_\mathrm{cur} > v_\mathrm{best}$ **then**
    $v_\mathrm{best} := v_\mathrm{cur}$
    $\widehat{\mathbf{i}^\star}(\mathbf{\Phi}) := \widehat{\mathbf{i}}(\mathbf{\Phi}, \theta_j)$
  end if
end for

Output: $\widehat{\mathbf{i}^\star}(\mathbf{\Phi})$

Algorithm 2

Input: $\mathbf{r}_{1:N_\mathrm{s}} = \left[\mathbf{r}_1^\top \ \mathbf{r}_2^\top \ \ldots \ \mathbf{r}_{N_\mathrm{s}}^\top\right]^\top, M$

1: $j := 1$

2: **for** $\mathbf{\Phi} \in \mathcal{W}_M \times \mathcal{W}_M$ **do**

3: $\widehat{\mathbf{i}}_j^\star = \text{GLRT\_Sequence\_Detection\_Given\_}\mathbf{\Phi}(\mathbf{r}_{1:N_\mathrm{s}}, \mathbf{\Phi})$

4: $v_j := \left|\left(\mathbf{r}_{1:N_\mathrm{s}}\right)^\mathrm{H} \mathbf{x}_{\widehat{\mathbf{i}}_j^\star}(\mathbf{\Phi})\right|$

5: $j := j + 1$

6: **end for**

7: $j^\star := \arg \max_{j \in \{1,2,\ldots,M^2\}} v_j$

Output: $\widehat{\mathbf{i}}_{j^\star}^\star$

1) Encoding: The transmitter encodes a sequence of K information bits to a sequence of $N_\mathrm{c} \geq K$ coded bits through a linear function over the binary field. Specifically, a linear block code $\mathcal{C}$ over the field $\mathbb{B}$ is a K-dimensional subspace of $\mathbb{B}^{N_\mathrm{c}}$. A binary N_c-tuple is a codeword of $\mathcal{C}$ if and only if there exists a binary K-tuple that can generate this N_c-tuple from $\mathbf{G}$, i.e.,[3]

$$\mathbf{c} \in \mathcal{C} \Longleftrightarrow \exists\ \mathbf{b} \in \mathbb{B}^K : \mathbf{c} = \mathbf{b}\mathbf{G}. \tag{48}$$

The ratio $R^\mathcal{C} \triangleq \frac{K}{N_\mathrm{c}}$ defines the rate of the code $\mathcal{C}$, while the minimum distance $d_{\min}^\mathcal{C}$ of $\mathcal{C}$ is the smallest Hamming weight w_H (i.e., the number of non-zero components) of any non-zero codeword in $\mathcal{C}$, i.e., $d_{\min}^\mathcal{C} = \min_{\mathbf{c} \in \mathcal{C} \setminus \{\mathbf{0}\}} \mathsf{w}_\mathrm{H}(\mathbf{c})$. Hereafter, a code will be abbreviated by the triplet $(N_\mathrm{c}, K, d_{\min}^\mathcal{C})$.

2) Soft-Decision Noncoherent Hybrid Composite Hypothesis-Testing (NC-HCHT) Decoding: As already mentioned, the tags are inherently resource-constrained and thus, utilization of small block-length channel codes is mandatory. However, a major obstacle for small block-length channel codes over wireless environments is the fact that errors usually occur in long bursts when the channel is in deep fade [31].[4] When wireless channel fading affects a sheer amount of bits, the use of channel codes with small block-length is not appropriate, due to their small

[3]All channel coding-related vectors are considered as row vectors, hereafter.

[4]As discussed in [37], in bistatic scatter radio, deep fading events are even more frequent due to the product of channel gain terms $a_\mathrm{CT}, a_\mathrm{TR}$.

error-correction capability. The interleaving technique in conjunction with linear block codes (of relatively small length, i.e., short packet) overcomes this difficulty [38].

The transmitter stores a block of D codewords in a $D\times N_{\mathrm{c}}$ matrix and transmits the information column-wise (where D is the interleaving depth of the interleaver), i.e., it transmits the first coded bit of each of the D codewords and then the second bit of each of the D codewords and so forth, until the N_{c}-th coded bit. The receiver stores DN_{c} received symbols and performs decoding row-wise, i.e., it decodes symbol sequences corresponding to actual codewords. In that way, the burst errors affect bits of different codewords, rather than consecutive bits of the same codeword [31]. It can be shown that a fully interleaved coded system (i.e., $DT \geq T_{\mathrm{coh}}$), with classic FSK and Rayleigh fading, achieves diversity order $d_{\min}^{\mathcal{C}}$ under ML noncoherent decoding [39].

For the scatter radio case, each tag backscatters a packet of DN_{c} coded bits. After DC-blocking, CFO estimation/compensation and symbol synchronization, SDR reader processes DN_{c} received symbols. Let $\mathbf{c} = [c_1 \ c_2 \ \ldots \ c_{N_{\mathrm{c}}}] \in \mathcal{C}$ be a codeword corresponding to a specific row of the interleaving matrix; according to (17), the discrete baseband signal, associated with that row of interleaving matrix, is given by:

$$\mathbf{r}_{1:N_{\mathrm{c}}} = \begin{bmatrix} \mathbf{r}_1 \\ \mathbf{r}_2 \\ \vdots \\ \mathbf{r}_{N_{\mathrm{c}}} \end{bmatrix} = \begin{bmatrix} h_1 \mathbf{x}_{c_1}(\mathbf{\Phi}) \\ h_2 \mathbf{x}_{c_2}(\mathbf{\Phi}) \\ \vdots \\ h_{N_{\mathrm{c}}} \mathbf{x}_{c_{N_{\mathrm{c}}}}(\mathbf{\Phi}) \end{bmatrix} + \begin{bmatrix} \mathbf{n}_1 \\ \mathbf{n}_2 \\ \vdots \\ \mathbf{n}_{N_{\mathrm{c}}} \end{bmatrix}, \tag{49}$$

where $\mathbf{r}_n$ and $\mathbf{x}_{c_n}(\mathbf{\Phi})$ are defined as in Section III-B, $c_n \in \mathbb{B}$, $n = 1, 2, \ldots, N_{\mathrm{c}}$ and $\{h_n\}_{n=1}^{N_{\mathrm{c}}}$ are the channel coefficients associated with coded bits $\{c_n\}_{n=1}^{N_{\mathrm{c}}}$. The noise statistics are given as in Section III-B. In sharp contrast to Eq. (32), it is remarked that in Eq. (49): (a) the transmitted sequence $\mathbf{c}$ belongs to a linear subspace of $\mathbb{B}^{N_{\mathrm{c}}}$ and (b) some of $\{h_n\}_{n=1}^{N_{\mathrm{c}}}$ may be independent of each other, depending on the sequence length, interleaving depth, and channel coherence time. For the particular case of a fully interleaved system, i.e., $DT \geq T_{\mathrm{coh}}$, $\{h_n\}_{n=1}^{N_{\mathrm{c}}}$ are independent of each other and diversity gain can be obtained.[5]

As in the uncoded case, the ML decoding rule does not admit a closed form and thus, an alternative decoding rule should be designed. In this work, the notion of NC-HCHT decoding

[5]Statistical independence among channel coefficients $\{h_n\}_{n=1}^{N_{\mathrm{c}}}$ also implies that they are distinct (i.e., unequal), given that they are drawn from a *continuous* distribution.

is applied, treating Φ_0 and Φ_1 as uniform random variables in $[0, 2\pi)$ and $\{h_n\}_{n=1}^{N_\mathrm{c}}$ as unknown nonrandom parameters:

$$\arg\max_{\mathbf{c}\in\mathcal{C}} \left\{ \mathop{\mathbb{E}}_{\mathbf{\Phi}} \left[\max_{\mathbf{h}\in\mathbb{C}^{N_\mathrm{c}}} \ln\left[\mathsf{f}_{\mathbf{r}_{1:N_\mathrm{c}}|\mathbf{c},\mathbf{h},\mathbf{\Phi}}(\mathbf{r}_{1:N_\mathrm{c}}|\mathbf{c},\mathbf{h},\mathbf{\Phi}) \right] \right] \right\}, \tag{50}$$

where $\mathbf{h} = [h_1 \ h_2 \ \ldots \ h_{N_\mathrm{c}}]^\top$.

Theorem 2. For $DT \geq T_\mathrm{coh}$, the decoding rule in Eq. (50) is simplified to the following soft-decision, channel-agnostic rule:

$$\widehat{\mathbf{c}} = \arg\max_{\mathbf{c}\in\mathcal{C}} \sum_{n=1}^{N_\mathrm{c}} w_n c_n, \tag{51}$$

where $w_n \triangleq |r_1^+(n)|^2 + |r_1^-(n)|^2 - \left(|r_0^+(n)|^2 + |r_0^-(n)|^2\right)$, $n = 1, 2, \ldots, N_\mathrm{c}$.

Proof. Due to the conditional independence of each $\mathbf{r}_n$ given the transmitted codeword $\mathbf{c}$ and the parameters $\mathbf{h}, \Phi_0, \Phi_1$, the log-likelihood PDF can be factorized as:

$$\sum_{n=1}^{N_\mathrm{c}} \ln\left[\mathsf{f}_{\mathbf{r}_n|c_n,h_n,\mathbf{\Phi}}(\mathbf{r}_n|c_n,h_n,\mathbf{\Phi}) \right]. \tag{52}$$

Hence, the log-likelihood PDF is a separable function of $\{h_n\}_{n=1}^{N_\mathrm{c}}$. Given that the channel coefficients $\{h_n\}_{n=1}^{N_\mathrm{c}}$ are statistically independent and distinct (due to $DT \geq T_\mathrm{coh}$), the innermost maximization in (50) can be expressed as the sum of independent maximizations:

$$\begin{aligned} &\max_{\mathbf{h}\in\mathbb{C}^{N_\mathrm{c}}} \ln\left[\mathsf{f}_{\mathbf{r}_{1:N_\mathrm{c}}|\mathbf{c},\mathbf{h},\mathbf{\Phi}}(\mathbf{r}_{1:N_\mathrm{c}}|\mathbf{c},\mathbf{h},\mathbf{\Phi}) \right] = \\ &\sum_{n=1}^{N_\mathrm{c}} \max_{h_n\in\mathbb{C}} \ln\left[\mathsf{f}_{\mathbf{r}_n|c_n,h_n,\mathbf{\Phi}}(\mathbf{r}_n|c_n,h_n,\mathbf{\Phi}) \right]. \end{aligned} \tag{53}$$

Each individual maximization can be calculated as in Lemma 1 through Eq. (24). Applying expectation with respect to Φ_0 and Φ_1 in (53), the following is obtained:

$$\begin{aligned} &\mathop{\mathbb{E}}_{\mathbf{\Phi}} \left[\sum_{n=1}^{N_\mathrm{c}} \left[Q^{(n)} + A_{c_n}^{(n)} \right] \right] = \sum_{n=1}^{N_\mathrm{c}} \mathop{\mathbb{E}}_{\mathbf{\Phi}} \left[Q^{(n)} + A_{c_n}^{(n)} \right] \\ &= \sum_{n=1}^{N_\mathrm{c}} \left(Q^{(n)} + (1-c_n) \mathop{\mathbb{E}}_{\mathbf{\Phi}} \left[A_0^{(n)} \right] + c_n \mathop{\mathbb{E}}_{\mathbf{\Phi}} \left[A_1^{(n)} \right] \right) \\ &= \sum_{n=1}^{N_\mathrm{c}} \left(Q^{(n)} + \mathop{\mathbb{E}}_{\mathbf{\Phi}} \left[A_0^{(n)} \right] + c_n \left(\mathop{\mathbb{E}}_{\mathbf{\Phi}} \left[A_1^{(n)} \right] - \mathop{\mathbb{E}}_{\mathbf{\Phi}} \left[A_0^{(n)} \right] \right) \right), \end{aligned} \tag{54}$$

where

$$A_{c_n}^{(n)} = \frac{1}{N_0}\left(|r_{c_n}^{+}(n)|^2 + |r_{c_n}^{-}(n)|^2\right) + \frac{2}{N_0}\Re\left\{(r_{c_n}^{+}(n))^*(r_{c_n}^{-}(n))\mathsf{e}^{2\mathsf{j}\Phi_{c_n}}\right\}. \quad (55)$$

$$Q^{(n)} = 4\mathsf{ln}\left(\frac{2}{\pi N_0}\right) - \frac{2}{N_0}||\mathbf{r}_n||_2^2. \quad (56)$$

According to Eq. (25), for any $n = 1, 2, \ldots, N_{\rm c}$,

$$\mathop{\mathbb{E}}_{\mathbf{\Phi}}\left[A_{c_n}^{(n)}\right] = \frac{1}{N_0}\left(|r_{c_n}^{+}(n)|^2 + |r_{c_n}^{-}(n)|^2\right). \quad (57)$$

Ignoring the terms in Eq. (54) that do not affect the outer maximization, the rule in Eq. (50) is simplified to:

$$\widehat{\mathbf{c}} = \arg\max_{\mathbf{c}\in\mathcal{C}}\left\{\sum_{n=1}^{N_{\rm c}} c_n\left(\mathop{\mathbb{E}}_{\mathbf{\Phi}}\left[A_1^{(n)}\right] - \mathop{\mathbb{E}}_{\mathbf{\Phi}}\left[A_0^{(n)}\right]\right)\right\}, \quad (58)$$

completing the proof. □

The receiver forms the vector $\mathbf{w} = \{w_n\}_{n=1}^{N_{\rm c}}$ of "soft decisions" for each row of interleaving matrix and applies the rule in (51) D times. Soft-decision decoding offers smaller BER performance compared to hard-decision decoding, where the receiver applies first detection on a symbol-by-symbol basis and then applies decoding on the bit sequence.

The optimization problem in (51) enjoys exponential complexity, due to the exhaustive search over 2^K possible $N_{\rm c}$-tuples of set $\mathcal{C}$; relatively small block-length $N_{\rm c}$ (and thus small K) is utilized in practice. For simulation results, small block-length, cyclic Bose-Chaudhuri-Hocquenghem (BCH), as well as Reed-Muller (RM) channel codes are studied [40].

IV. Simulation Results

Simulations for the bistatic scatter radio system model assume backscatter binary FSK transmissions at $T = 1$ msec bitrate, over quasi-static flat fading channel with coherence time $T_{\rm coh} = 100$ msec; Rayleigh fading ($\kappa_{\rm CT} = \kappa_{\rm TR} = 0$), Rician fading with $\kappa_{\rm CT} = 20, \kappa_{\rm TR} = 10$ and no fading, i.e., Gaussian channel ($\kappa_{\rm CT} = \kappa_{\rm TR} \longrightarrow \infty$) are studied.[6] In all simulated cases, perfect symbol synchronization and CFO estimation/compensation are also assumed. For comparison

[6]Such coherence time and fading parameter values have been experimentally verified for immobile outdoor setups, CE close to tag and tag-reader distance more than 100 meters [16], [18] .

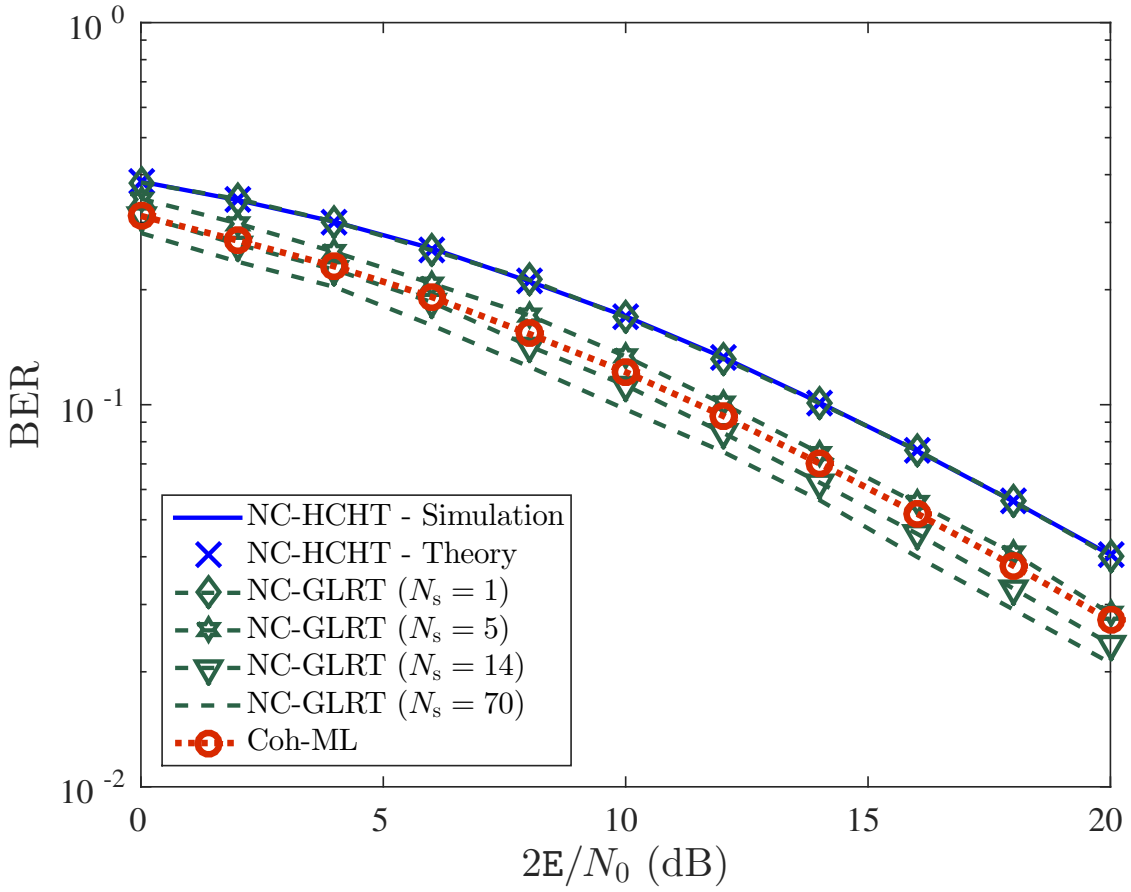

Fig. 2. BER vs average received SNR for Rayleigh fading with no channel coding of the various noncoherent detectors. Comparison to the coherent case is conducted for fixed energy per packet, including energy spent for channel estimation.

purposes, coherent detection and decoding schemes are also included with $N_{\rm tr} = 30$ training bits for channel estimation. In all cases, the average received SNR per information bit is given by Eq. (16), while packet length and energy consumption *per transmitted packet* are both fixed for comparison fairness. Hence, noncoherent receivers (with no dedicated training bits in the packet for channel estimation) have higher energy per information bit than their coherent counterparts, for equal packet lengths.

A. Uncoded BER Performance

For uncoded bistatic scatter radio system, the proposed noncoherent symbol-by-symbol and sequence detectors are compared to the ML coherent detector with least-squares (LS) channel estimation (abbreviated as Coh-ML) [18], assuming packets with 70 information bits for all setups. Thus, the total energy per packet is $70\mathtt{E}$ and $(30+70)\mathtt{E}$ for noncoherent and coherent

setup, respectively, taking into account the $N_{\rm tr} = 30$ training bits for channel estimation in the coherent case. For fixed energy per packet, the total energy per bit for noncoherent and coherent setup is $\mathtt{E}$ and $\frac{7}{10}\mathtt{E}$ Joules, respectively. Furthermore, $M = 6$ is employed for NC-GLRT sequence detection (for sequence length $N_{\rm s} \geq 2$).

Fig. 2 depicts for Rayleigh fading the BER of noncoherent symbol-by-symbol HCHT and GLRT detectors, GLRT sequence detector (for various sequence lengths $N_{\rm s}$), and Coh-ML detector. It is observed that for symbol-by-symbol NC-HCHT detection, simulation results and analytical expression of Eq. (26) perfectly match. Coh-ML detector outperforms by 2-3dB the symbol-by-symbol noncoherent detectors. For value of M as little as 6, increasing sequence length $N_{\rm s}$ of NC-GLRT sequence detector significantly improves BER performance, exhibiting 1-2dB performance gain compared to Coh-ML detector; it is remarked that under a constant energy consumption per packet, the energy per information bit in the coherent case is 30% smaller compared to the noncoherent case, due to the overhead spent on training bits (in the coherent case) for channel estimation. The NC-GLRT sequence detector capitalizes upon that, exploiting correlation (due to the unknown channel) between consecutive symbols and offers blind detection, i.e., no requirement for overhead (training) channel estimation bits. The performance increase of noncoherent sequence detector comes at the cost of slightly higher computational cost (requiring $\mathcal{O}(N_{\rm s}\log N_{\rm s})$ arithmetic operations) compared to noncoherent symbol-by-symbol and coherent detection schemes that require $\mathcal{O}(N_{\rm s})$ computational cost.[7] It is also noted that increasing parameter M beyond 6, offers negligible extra performance gain for the NC-GLRT sequence detector.

Fig. 3 compares the BER performance of NC-HCHT and Coh-ML detectors for different types of fading as a function of average received SNR. It is noted that the average received SNR in Eq. (16) is common in all fading scenarios considered. It can be seen that as parameters $\kappa_{\rm CT}$ and $\kappa_{\rm TR}$ increase, i.e., the channel becomes more deterministic, the BER gap between the two detection schemes is reduced with increasing SNR. It is observed that as the fading becomes more deterministic, the power gain dominates the BER performance in moderate and high SNR regime. Interestingly, for the Gaussian channel case (no fading, deterministic channel), NC-HCHT detector outperforms Coh-ML detector for SNR values greater than 12. As discussed

[7]Additionally, coherent detection requires extra $\mathcal{O}(N_{\rm tr}^3)$ arithmetic operations to obtain the LS estimate of the channel [18, Eq. (24)].

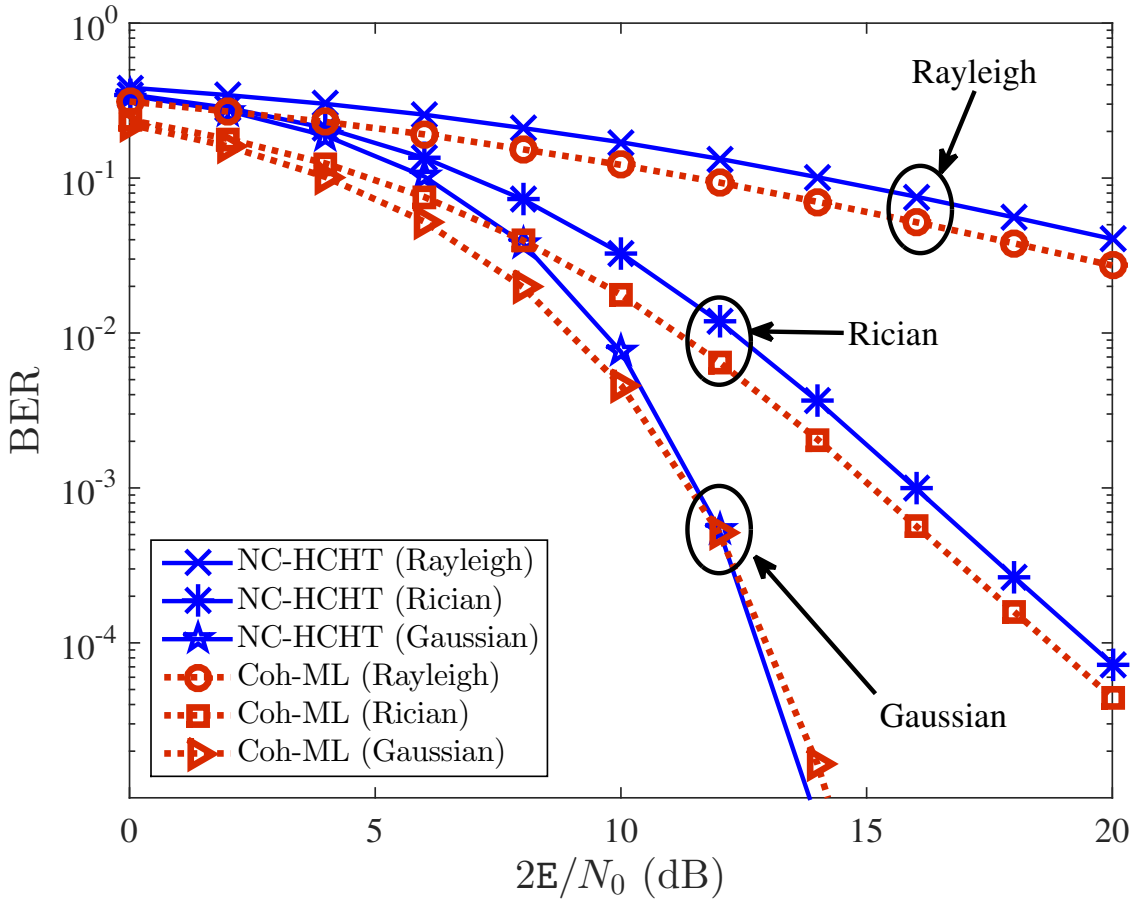

Fig. 3. BER vs average received SNR of NC-HCHT and Coh-ML detection for different fading scenarios. Comparison to the coherent case is conducted for fixed energy per packet, including energy spent for channel estimation.

above, this stems from the fact that noncoherent schemes have a higher power gain (E vs $\frac{7}{10}\mathrm{E}$ Joules per bit) compared to coherent one. This is highly important in typical scatter radio scenarios, with strong line-of-sight (LOS).

Fig. 4 studies the sequence length of NC-GLRT in various fading scenarios; as fading becomes more deterministic, the performance gap between NC-GLRT sequence detector and Coh-ML detector slightly increases, showing that the proposed log-linear complexity sequence detector is a promising option for power-limited scatter radio networks. It is emphasized again that the BER performance gain of noncoherent receivers also exploits the higher energy per information bit, compared to the coherent receiver, due to fixed energy per packet and no need for training/overhead bits for channel estimation. Both Fig. 3 and Fig. 4 above clearly indicate that the choice of preferable noncoherent detection scheme depends on the specifics of the wireless

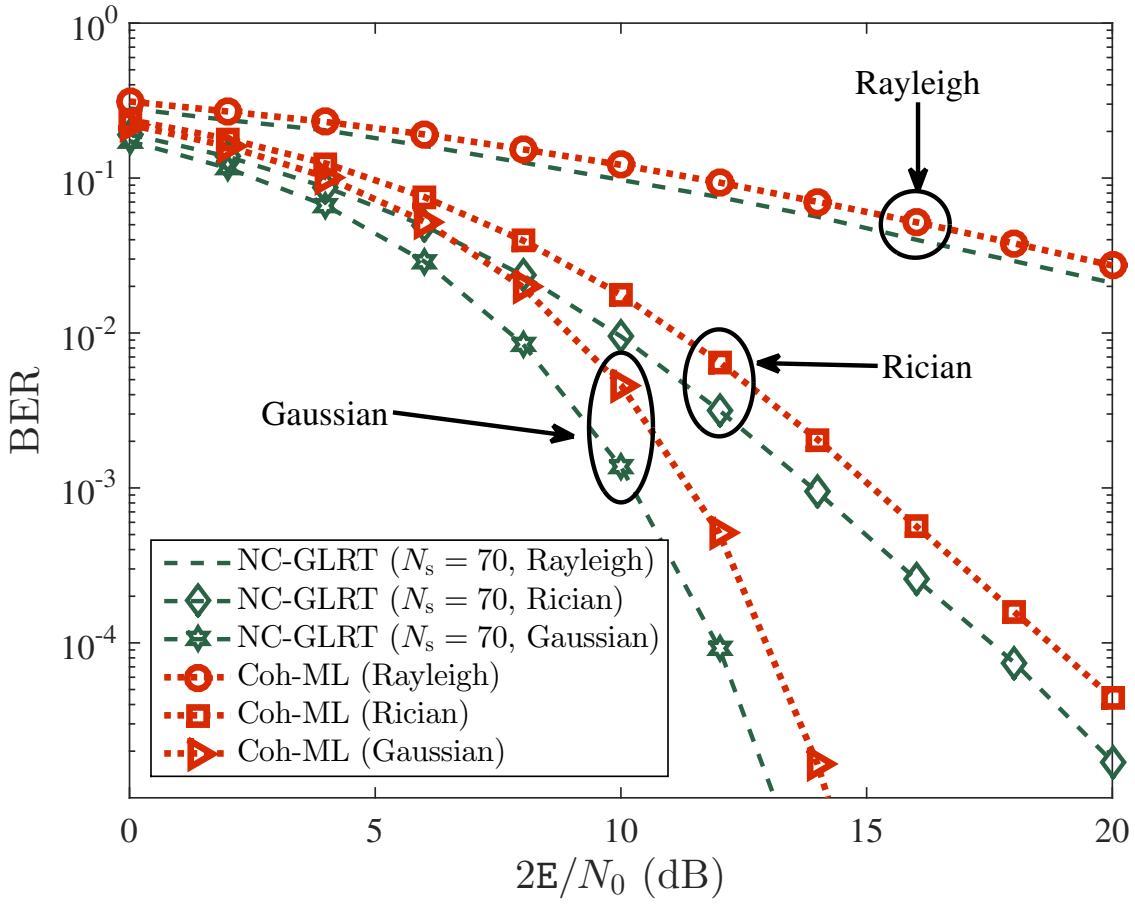

Fig. 4. Performance of GLRT sequence detection with $N_s = 70$ and Coh-ML detection for different fading scenarios and no channel coding. Comparison to the coherent case is conducted for fixed energy per packet, including energy spent for channel estimation.

fading channel and the SNR operating value.

B. Coded BER Performance

Using code $\mathcal{C}(N_c, K, d^{\mathcal{C}}_{\min})$ along with interleaving, the proposed NC-HCHT decoder of Eq. (51) and the ML coherent decoder with LS channel estimation (Coh-ML) [18] are compared in terms of BER. Two small block-length channel codes are studied: the cyclic $(31, 11, 11)$ BCH code $\mathcal{C}_{\mathrm{BCH}}$ and the $(32, 16, 8)$ RM channel code $\mathcal{C}_{\mathrm{RM}}$; the first has smaller rate but higher error-correction capability than the second. As in the uncoded case, a total energy budget constraint per packet is considered assuming packets of DN_c coded bits (i.e., $(K/N_c)DN_c$ information bits). Thus, for noncoherent coded setups the total energy per packet is $DN_c x$, where x is the energy cost per bit, while for coherent coded setups the total energy per packet

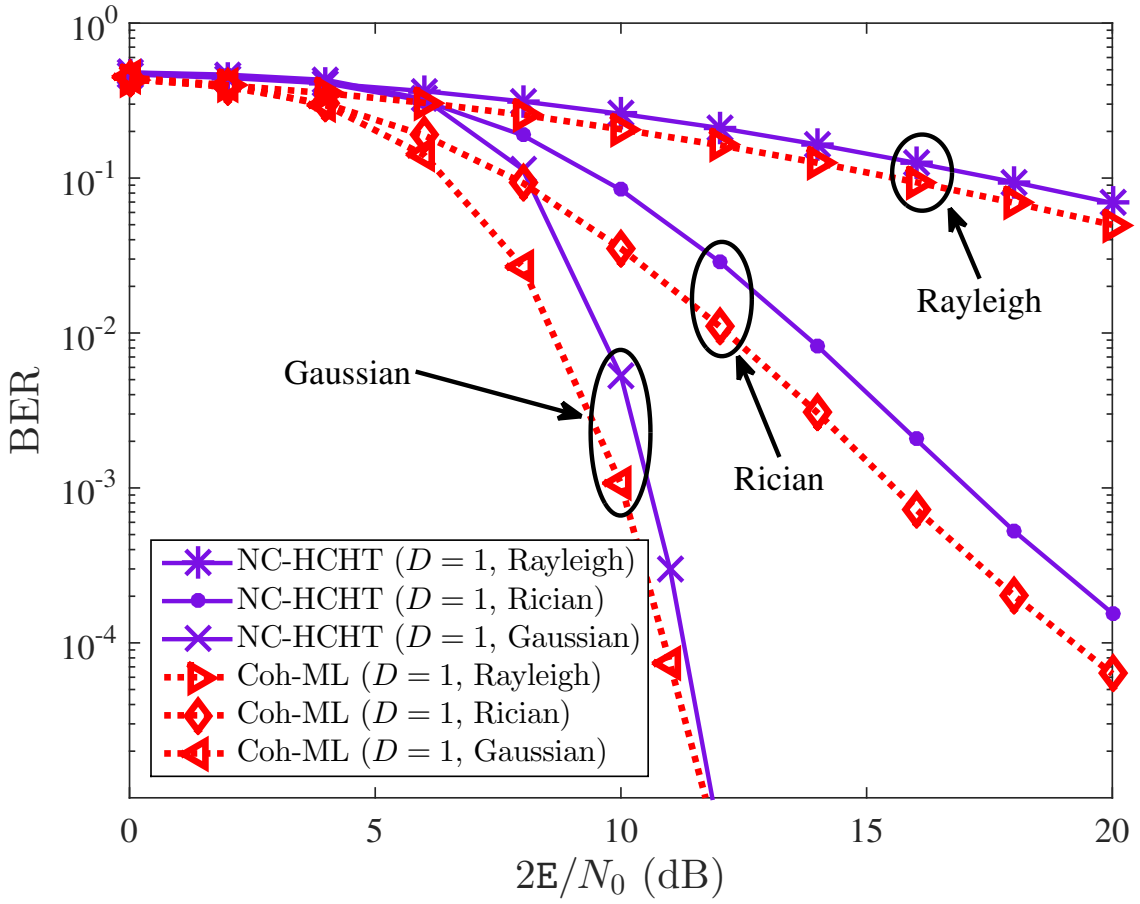

Fig. 5. Impact of fading in BER performance for HCHT and Coh-ML decoders. Both setups utilize the cyclic $(31, 11, 11)$ BCH code and $D = 1$. Comparison to the coherent case is conducted for fixed energy per packet, including energy spent for channel estimation.

is $[DN_{\rm c} + L_{\rm coh}N_{\rm tr}]\, x$, where integer $L_{\rm coh} \triangleq \left\lceil \dfrac{DN_{\rm c}T}{T_{\rm coh}} \right\rceil$ indicates how many times the channel needs to be estimated (utilizing $N_{\rm tr}$ training bits each time). Thus, for fixed energy per packet, i.e., $DN_{\rm c}x = (K/N_{\rm c})DN_{\rm c}\mathtt{E}$ or $[DN_{\rm c} + L_{\rm coh}N_{\rm tr}]\, x = (K/N_{\rm c})DN_{\rm c}\mathtt{E}$, the total energy per bit x for noncoherent and coherent coded setup is $\frac{K}{N_{\rm c}}\mathtt{E}$ and $\dfrac{KD}{DN_{\rm c} + L_{\rm coh}N_{\rm tr}}\mathtt{E}$ Joules, respectively.

Fig. 5 considers the use of $(31, 11, 11)$ BCH channel code with $D = 1$, i.e., no interleaving and studies the impact of fading in NC-HCHT and Coh-ML decoders. It can be seen that as fading parameters $\kappa_{\rm CT}, \kappa_{\rm TR}$ decrease, the BER for both decoding schemes increases. That is due to the higher randomness of fading for smaller values of $\kappa_{\rm CT}$ and $\kappa_{\rm TR}$ and the limited error-correction capability due to the small block-length of the utilized codes. It is also noted that as $\kappa_{\rm CT}, \kappa_{\rm TR}$ and SNR increase, the BER gap between the two schemes decreases.

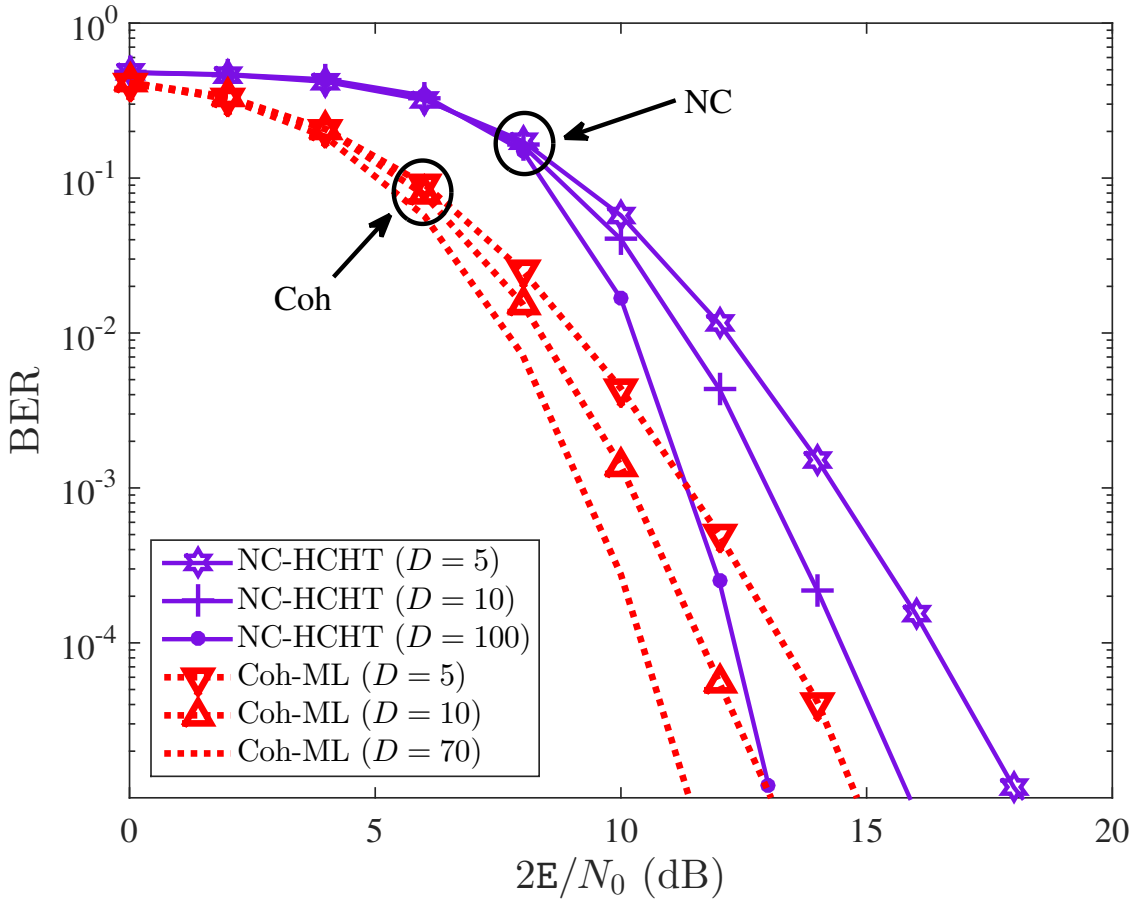

Fig. 6. Impact of interleaving depth D for NC-HCHT and Coh-ML decoders with cyclic $(31, 11, 11)$ BCH code over Rician fading. Comparison to the coherent case is conducted for fixed energy per packet, including energy spent for channel estimation.

Fig. 6 studies the impact of interleaving depth D in BCH NC-HCHT and Coh-ML decoders over Rician fading; as expected, the BER of both schemes is reduced with increasing D, due to the diversity gain introduced by interleaving. It is noted that for $D = 5$, Coh-ML decoder offers approximately 3 dB performance gain compared to NC-HCHT decoder. However, as D increases, their BER performance gap becomes smaller.

Finally, Fig. 7 compares the $(31, 11, 11)$ BCH cyclic and the $(32, 16, 8)$ RM channel codes for different fading scenarios, with NC-HCHT decoding and full interleaving. An interesting observation emerges: while for Rayleigh fading BCH-coded outperforms RM-coded system, for Rician fading they offer similar BER performance, whereas for no fading RM offers slightly smaller BER compared to BCH. This means that when κ_{CT} and κ_{TR} are small, i.e., in highly random fading scenarios, diversity gain (that depends on $d^{\mathrm{e}}_{\mathrm{min}}$) plays more important role in

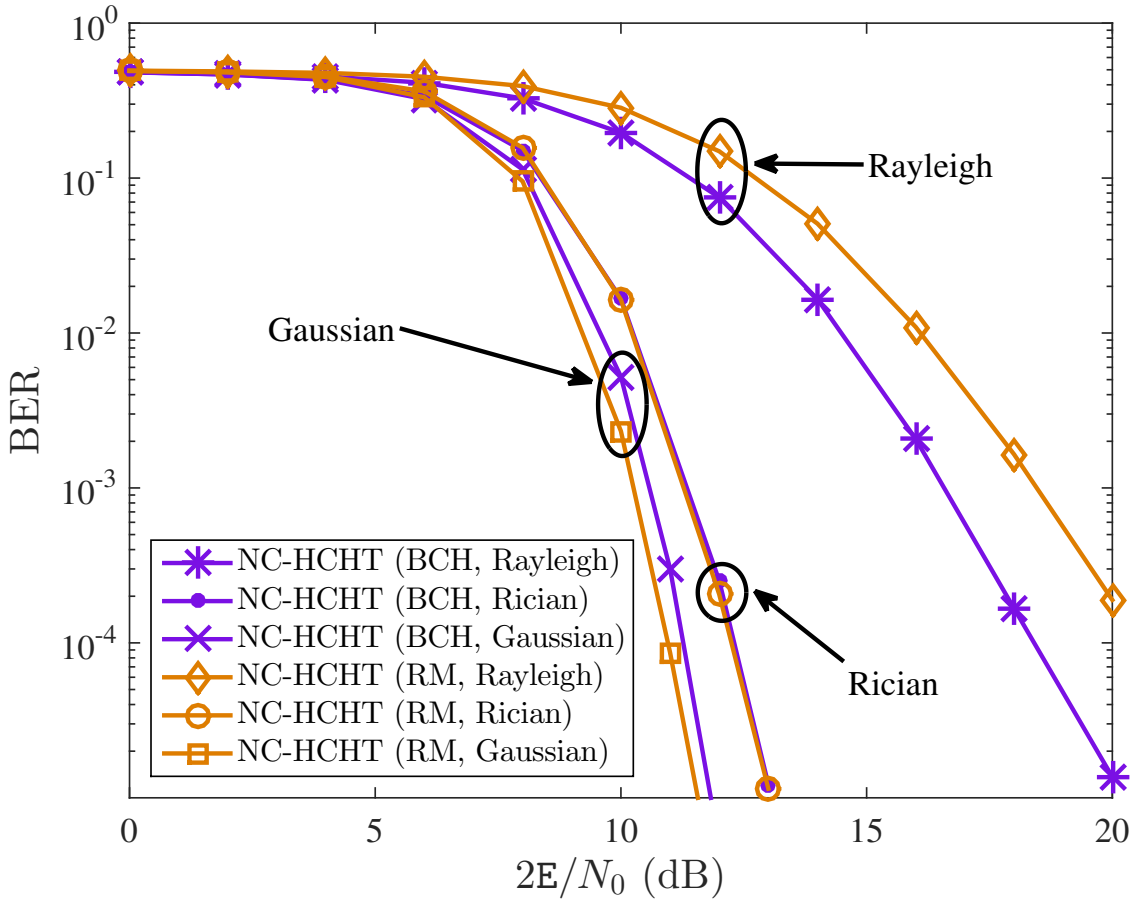

Fig. 7. Impact of fading for NC-HCHT decoder with cyclic $(31, 11, 11)$ BCH or $(32, 16, 8)$ RM channel code and full interleaving.

BER performance than energy gain (that depends on R^{c}), while the opposite holds in more deterministic fading scenarios.

V. Experimental Results

Outdoors measurements were conducted with the experimental setup of Fig. 8. An embedded carrier emitter (CE) was employed at frequency of 868 MHz and transmit power of 13 dBm. A custom 8-bit microcontroller-based, scatter radio tag was utilized at 1 kbps with binary FSK and switching (subcarrier) frequencies of $F_0 = 125$ kHz and $F_1 = 250$ kHz. A commodity (USRP2) SDR with Flex-900 front-end radio card was utilized as the receiver, connected to a laptop running the noncoherent and coherent detection/decoding algorithms. All radio modules were equipped with omni-directional antennas, at height of 1.70 meters. Channel coherence time of 50

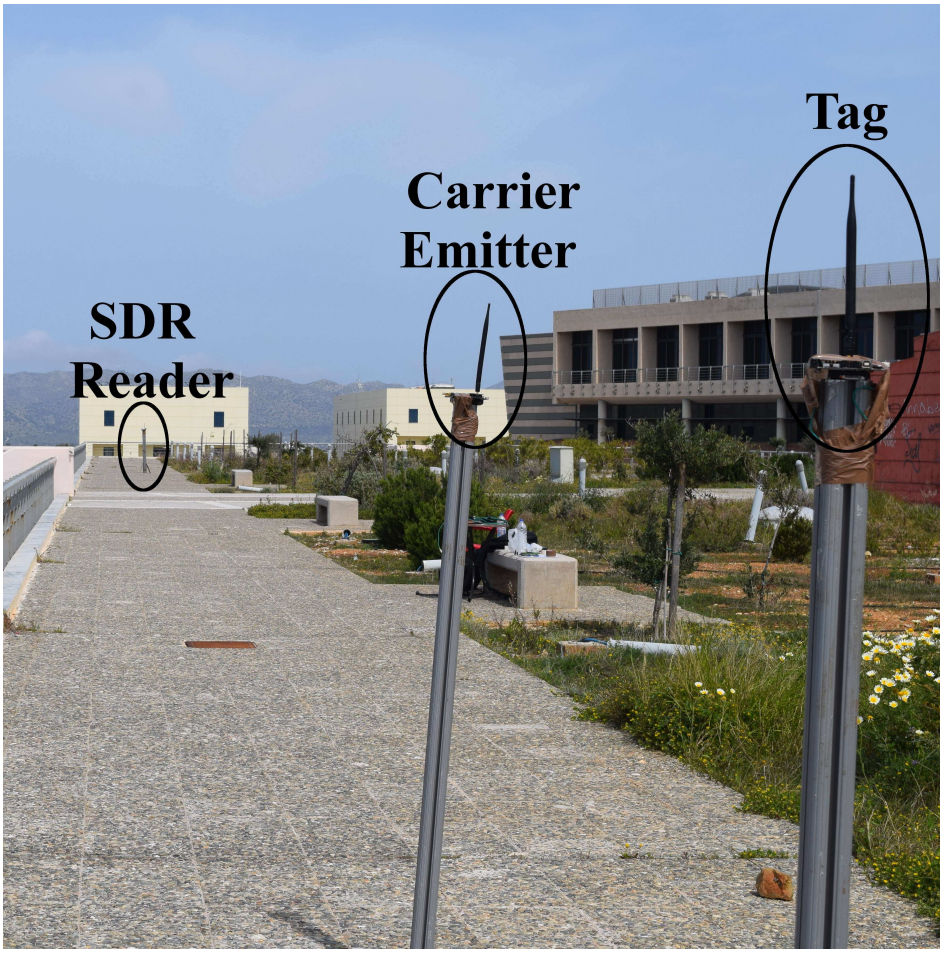

Fig. 8. Experimental, outdoor topology; depicted carrier emitter-to-tag distance d_{CT} was 8 meters.

to 100 msec was observed during the experimental results, due to immobility. For the considered experimental scenario, CE was placed between tag and SDR reader, co-linearly (Fig. 8).

A packet of 47 bits was utilized for both coherent and noncoherent setups. Periodogram-based CFO estimation was applied using the whole received signal,[8] and energy-based symbol and packet synchronization was also employed. The (last) 31 bits constitute a BCH codeword (i.e., $N_{\mathrm{c}} = 31$), utilized at both coherent and noncoherent setups for detection and decoding, while the remaining 16 bits were exploited only at the coherent case, for LS channel estimation. The following schemes were compared in terms of BER: (a) uncoded NC-HCHT symbol-by-symbol detector, (b) uncoded GLRT symbol-by-symbol detector, (c) uncoded GLRT sequence detector

[8]The periodogram is the maximum-likelihood estimate (MLE) of ΔF, whose mean-squared error (MSE) decays asymptotically with the cubic power of the number of utilized samples [41].

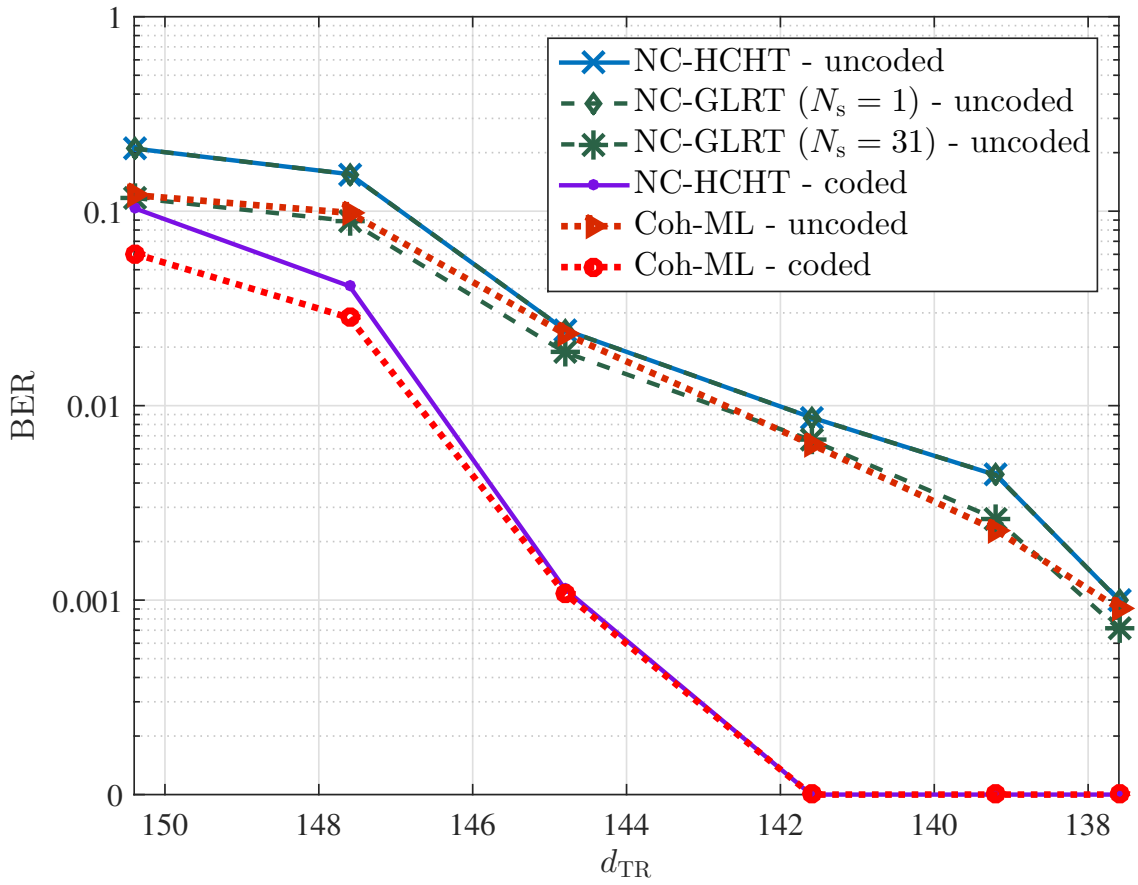

Fig. 9. Experimental BER comparison of all scatter radio receivers as a function of tag-to-SDR reader distance d_{TR} (m).

with $N_{\mathrm{s}} = 31$ and $M = 6$, (d) uncoded Coh-ML detector, (e) coded NC-HCHT decoder, and (f) coded Coh-ML decoder. $D = 1$ was utilized, i.e., coding schemes did not utilize interleaving. In addition, the energy per bit was held fixed, i.e., total energy per packet was not fixed among the different schemes (favoring coded vs uncoded or coherent vs noncoherent reception).

Fig. 9 offers the experimental BER of the above schemes as a function of the tag-to-reader distance. It can be seen that both coherent and noncoherent uncoded receivers achieve ranges in the order of 145m with BER $\leq 3\%$, while coded receivers achieve ranges of 148 and 141 meters approximately, at BER $\leq 4\%$ and 0, respectively. It is observed that uncoded coh-ML detector offers similar BER with uncoded (noncoherent) GLRT sequence detector and both of them outperform by approximately one meter the symbol-by-symbol noncoherent detectors (under unequal total energy cost per packet). Interestingly, it can be shown that the proposed noncoherent coded receiver achieves comparable BER performance with the coded coherent

one, even though the latter spends extra bits (and energy) for channel estimation; thus, potential energy gains are available for the noncoherent setup. It is worth emphasizing that the reported BER, in the order of 1%–5%, is acceptable for low bitrate sensing applications.

VI. Conclusions

This work offered novel noncoherent reception schemes for scatter radio FSK, channel-coded or not, ideal for short packet communication under energy budget constrains and Rician, Rayleigh or no fading. The focus was on scatter radio FSK, in order to enable frequency-division multiplexing and collision-free networking of several (possible receiver-less) tags/sensors. Perhaps, this work may spark additional interest in the adoption of ultra-low complexity and power scatter radio for future low-cost, possibly ambiently powered WSNs and relevant Internet-of-Things applications.

Appendix A
Proof of Proposition 1

Given hypothesis $i=0$ and h,Φ_0,Φ_1, random variable (RV) $z_1 \triangleq |r_1^+|^2+|r_1^-|^2$ is the sum of 4 independent, squared, zero-mean Gaussians, each of variance $\sigma^2 \triangleq N_0/4$ and thus, z_1 follows a Chi-squared distribution with 4 degrees of freedom and probability density function (PDF) given by [39, p. 45]: $\mathsf{f}_{z_1|i}(x|0)=\frac{x}{4\sigma^4}\mathsf{e}^{-\frac{x}{2\sigma^2}},\quad x\geq 0$, and corresponding cumulative distribution function (CDF) given by:

$$\mathsf{F}_{z_1|i}(x|0)=1-\mathsf{e}^{-\frac{x}{2\sigma^2}}\left(1+\frac{x}{2\sigma^2}\right),\ x\geq 0. \tag{59}$$

Similarly, given hypothesis $i=0$ and h,Φ_0,Φ_1, random variable $z_0 \triangleq |r_0^+|^2+|r_0^-|^2$ is the sum of 4 independent squared non-zero-mean Gaussian RVs, each of variance σ^2 and thus, z_0 follows noncentral Chi-squared with 4 degrees of freedom with noncentrality parameter $\mathtt{E}\,|h|^2=\mathtt{E}\,a^2$ that do not depend on RV Φ_0. The conditional PDF of z_0 is given by [39, p. 46]:

$$\mathsf{f}_{z_0|i,a}(x|0,a)=\frac{\sqrt{x}}{2\sigma^2\sqrt{\mathtt{E}}\,a}\mathsf{e}^{-\frac{x+\mathtt{E}\,a^2}{2\sigma^2}}\mathsf{I}_1\left(a\frac{\sqrt{x\,\mathtt{E}}}{\sigma^2}\right),x\geq 0, \tag{60}$$

where $\mathsf{I}_1(\cdot)$ is the modified Bessel of the first kind and order one [39, p. 47].

Under hypothesis $i=0$, error occurs if $z_0<z_1$. Applying the law of iterated expectation [42], the probability of that event can be calculated as follows:

$$\Pr(e|i=0)=\Pr(z_1>z_0|i=0)=\mathop{\mathbb{E}}_{a}\left[\mathop{\mathbb{E}}_{z_0|a,i=0}\left[1-\mathsf{F}_{z_1|i}(z_0|0)\right]\right]. \tag{61}$$

In view of Eq. (59), the inner expectation in Eq. (61) is given by:

$$\begin{aligned}
&\mathop{\mathbb{E}}_{z_0|a,i=0}\left[1-\mathsf{F}_{z_1|i}(z_0|0)\right]\\
&=\int_0^{+\infty}\left(1-\mathsf{F}_{z_1|i}(x|0)\right)\mathsf{f}_{z_0|i,a}(x|0,a)\mathsf{d}x\\
&=\int_0^{+\infty}\frac{\left(1+\frac{x}{2\sigma^2}\right)\sqrt{x}}{2\sigma^2\sqrt{\mathtt{E}}\,a}\mathsf{e}^{-\frac{2x+\mathtt{E}\ a^2}{2\sigma^2}}\mathsf{I}_1\left(\frac{a\sqrt{\mathtt{E}\,x}}{\sigma^2}\right)\mathsf{d}x \qquad (62)\\
&=\frac{\mathsf{e}^{-\frac{\mathtt{E}\ a^2}{4\sigma^2}}\left(\mathtt{E}\ a^2+16\sigma^2\right)}{32\sigma^2}, \qquad (63)
\end{aligned}$$

where [43, Eq. (6.643.2)] was used to evaluate the integral in Eq. (62) and [35, Eqs. (13.15.1), (13.18.3)] were exploited to simplify and obtain Eq. (63).

Substituting $\mathtt{SNR}=\mathtt{E}/(2\sigma^2)$ in Eq. (63), and applying expectation with respect to $a=a_{\mathrm{CT}}a_{\mathrm{TR}}$ under independent Rayleigh fading, offers the following:

$$\begin{aligned}
&\mathop{\mathbb{E}}_{a}\left[\frac{\mathsf{e}^{-\frac{\mathtt{E}\ a^2}{4\sigma^2}}\left(\mathtt{E}\ a^2+16\sigma^2\right)}{32\sigma^2}\right]=\mathop{\mathbb{E}}_{a}\left[\mathsf{e}^{-\frac{\mathtt{SNR}\ a^2}{2}}\left(\frac{\mathtt{SNR}\ a^2}{16}+\frac{1}{2}\right)\right]\\
&=\mathop{\mathbb{E}}_{a_{\mathrm{CT}}}\left[\mathop{\mathbb{E}}_{a_{\mathrm{TR}}}\left[\mathsf{e}^{-\frac{(a_{\mathrm{CT}}a_{\mathrm{TR}})^2\ \mathtt{SNR}}{2}}\left(\frac{(a_{\mathrm{CT}}a_{\mathrm{TR}})^2\ \mathtt{SNR}}{16}+\frac{1}{2}\right)\right]\right] \qquad (64)\\
&=\int_0^{\infty}\int_0^{\infty}4\ x\ y\ \mathsf{e}^{-x^2-y^2-\frac{(xy)^2\ \mathtt{SNR}}{2}}\left(\frac{(xy)^2\ \mathtt{SNR}}{16}+\frac{1}{2}\right)\mathsf{d}x\mathsf{d}y\\
&=\int_0^{\infty}y\,\mathsf{e}^{-y^2}\frac{8+5y^2\mathtt{SNR}}{2\left(y^2\mathtt{SNR}+2\right)^2}\mathsf{d}y \qquad (65)\\
&=\frac{\mathsf{e}^{\frac{2}{\mathtt{SNR}}}}{4\mathtt{SNR}^2}\int_{\frac{2}{\mathtt{SNR}}}^{\infty}\mathsf{e}^{-y}\frac{-2+5y\mathtt{SNR}}{y^2}\mathsf{d}y \qquad (66)\\
&=\frac{\mathsf{e}^{\frac{2}{\mathtt{SNR}}}\left(5\mathtt{SNR}+2\right)\mathsf{E}_1\left(\frac{2}{\mathtt{SNR}}\right)}{4\mathtt{SNR}^2}-\frac{1}{4\mathtt{SNR}}, \qquad (67)
\end{aligned}$$

where [43, Eq. (3.461.3)] was exploited to derive Eq. (65), while Eq. (67) results from [43, Eq. (3.351.4)] and [35, Eq. (6.2.6)]. Due to symmetry, $\Pr(e|i=0)=\Pr(e|i=1)=\Pr(e)$ and the proof is completed.

REFERENCES

[1] G. Vannucci, A. Bletsas, and D. Leigh, "A software-defined radio system for backscatter sensor networks," *IEEE Trans. Wireless Commun.*, vol. 7, no. 6, pp. 2170–2179, Jun. 2008.

[2] K. Finkenzeller, *RFID Handbook: Fundamentals and Applications in Contactless Smart Cards and Identification*, 2nd ed. New York, NY, USA: John Wiley & Sons, Inc., 2003.

[3] A. Collado and A. Georgiadis, "Conformal hybrid solar and electromagnetic (EM) energy harvesting rectenna," *IEEE Trans. Circuits Syst. I*, vol. 60, pp. 2225–2234, Aug. 2013.

[4] S. Kim, C. Mariotti, F. Alimenti, P. Mezzanotte, A. Georgiadis, A. Collado, L. Roselli, and M. Tentzeris, "No battery required: perpetual RFID-enabled wireless sensors for cognitive intelligence applications," *IEEE Microw. Mag.*, vol. 14, no. 5, pp. 66–77, Jul. 2013.

[5] G. D. Durgin, "RF thermoelectric generation for passive RFID," in *Proc. IEEE Int. Conf. on RFID (RFID)*, Orlando, FL, May 2016, pp. 1–8.

[6] A. Bletsas, A. G. Dimitriou, and J. N. Sahalos, "Improving backscatter radio tag efficiency," *IEEE Trans. Microw. Theory Techn.*, vol. 58, no. 6, pp. 1502–1509, Jun. 2010.

[7] D. Kim, M. A. Ingram, and W. W. Smith, "Measurements of small-scale fading and path loss for long range RF tags," *IEEE Trans. Antennas Propag.*, vol. 51, no. 8, pp. 1740–1749, Aug. 2003.

[8] J. D. Griffin and G. D. Durgin, "Link envelope correlation in the backscatter channel," *IEEE Commun. Lett.*, vol. 11, no. 9, pp. 735–737, Sep. 2007.

[9] ——, "Gains for RF tags using multiple antennas," *IEEE Trans. Antennas Propag.*, vol. 56, no. 2, pp. 563–570, Feb. 2008.

[10] ——, "Complete link budgets for backscatter-radio and RFID systems," *IEEE Antennas Propag. Mag.*, vol. 51, no. 2, pp. 11–25, Apr. 2009.

[11] C. Angerer, R. Langwieser, and M. Rupp, "RFID reader receivers for physical layer collision recovery," *IEEE Trans. Commun.*, vol. 58, no. 12, pp. 3526–3537, Dec. 2010.

[12] A. Bletsas, J. Kimionis, A. G. Dimitriou, and G. N. Karystinos, "Single-antenna coherent detection of collided FM0 RFID signals," *IEEE Trans. Commun.*, vol. 60, no. 3, pp. 756–766, 2012.

[13] N. Kargas, F. Mavromatis, and A. Bletsas, "Fully-coherent reader with commodity SDR for Gen2 FM0 and computational RFID," *IEEE Wireless Commun. Lett.*, vol. 4, no. 6, pp. 617–620, Dec. 2015.

[14] J. Kimionis, A. Bletsas, and J. N. Sahalos, "Design and implementation of RFID systems with software defined radio," in *Proc. IEEE European Conf. on Antennas and Propagation (EuCAP)*, Prague, Czech Republic, Mar. 2012, pp. 3464–3468.

[15] ——, "Bistatic backscatter radio for power-limited sensor networks," in *Proc. IEEE Global Commun. Conf. (Globecom)*, Atlanta, GA, USA, Dec. 2013, pp. 353–358.

[16] ——, "Increased range bistatic scatter radio," *IEEE Trans. Commun.*, vol. 62, no. 3, pp. 1091–1104, Mar. 2014.

[17] P. N. Alevizos, N. Fasarakis-Hilliard, K. Tountas, N. Agadakos, N. Kargas, and A. Bletsas, "Channel coding for increased range bistatic backscatter radio: Experimental results," in *Proc. IEEE RFID Technology and Applications (RFID-TA)*, Tampere, Finland, Sep. 2014.

[18] N. Fasarakis-Hilliard, P. N. Alevizos, and A. Bletsas, "Coherent detection and channel coding for bistatic scatter radio sensor networking," *IEEE Trans. Commun.*, vol. 63, no. 5, pp. 1798–1810, May 2015.

[19] P. N. Alevizos, Y. Fountzoulas, G. N. Karystinos, and A. Bletsas, "Noncoherent sequence detection of orthogonally modulated signals in flat fading with log-linear complexity," in *Proc. IEEE Int. Conf. Acoustics, Speech, and Signal Processing (ICASSP)*, Brisbane, Australia, Apr. 2015, pp. 2974–2978.

[20] E. Kampianakis, J. Kimionis, K. Tountas, C. Konstantopoulos, E. Koutroulis, and A. Bletsas, "Wireless environmental sensor networking with analog scatter radio & timer principles," *IEEE Sensors J.*, vol. 14, no. 10, pp. 3365–3376, Oct. 2014.

[21] S. N. Daskalakis, S. D. Assimonis, E. Kampianakis, and A. Bletsas, "Soil moisture scatter radio networking with low power," *IEEE Trans. Microw. Theory Techn.*, vol. 64, no. 7, pp. 2338–2346, Jul. 2016.

[22] C. Konstantopoulos, E. Koutroulis, N. Mitianoudis, and A. Bletsas, "Converting a plant to a battery and wireless sensor with scatter radio and ultra-low cost," *IEEE Trans. Instrum. Meas.*, vol. 65, no. 2, pp. 388–398, Feb. 2016.

[23] V. Liu, A. Parks, V. Talla, S. Gollakota, D. Wetherall, and J. R. Smith, "Ambient backscatter: Wireless communication out of thin air," in *ACM SIGCOMM*, Hong Kong, China, 2013, pp. 39–50.

[24] J. F. Ensworth and M. S. Reynolds, "Every smart phone is a backscatter reader: Modulated backscatter compatibility with bluetooth 4.0 low energy (BLE) devices," in *Proc. IEEE Int. Conf. on RFID (RFID)*, San Diego, CA, Apr. 2015, pp. 78–85.

[25] G. Vougioukas, S. N. Daskalakis, and A. Bletsas, "Could battery-less scatter radio tags achieve 270-meter range?" in *Proc. IEEE Wireless Power Transfer Conf. (WPTC)*, Aveiro, Portugal, May 2016, pp. 1–3.

[26] A. Bletsas, S. Siachalou, and J. N. Sahalos, "Anti-collision backscatter sensor networks," *IEEE Trans. Wireless Commun.*, vol. 8, no. 10, pp. 5018–5029, Oct. 2009.

[27] K. Tountas, P. N. Alevizos, A. Tzedaki, and A. Bletsas, "Bistatic architecture provides extended coverage and system reliability in scatter sensor networks," in *Proc. International EURASIP Workshop on RFID Technology (EURFID)*, Rosenheim, Germany, Oct. 2015, pp. 144–151.

[28] Y. Polyanskiy, H. V. Poor, and S. Verdù, "Channel coding rate in the finite blocklength regime," *IEEE Trans. Inf. Theory*, vol. 56, no. 5, pp. 2307–2359, May 2010.

[29] G. Durisi, T. Koch, and P. Popovski, "Towards massive, ultra-reliable, and low-latency wireless communication with short packets," *Proc. IEEE*, vol. 104, no. 9, pp. 1711–1726, Sep. 2016.

[30] P. N. Alevizos and A. Bletsas, "Noncoherent composite hypothesis testing receivers for extended range bistatic scatter radio WSNs," in *Proc. IEEE Int. Conf. on Commun. (ICC)*, London, U.K., Jun. 2015.

[31] D. Tse and P. Viswanath, *Fundamentals of Wireless Communication*. New York: Cambridge University Press, 2005.

[32] A. Goldsmith, *Wireless Communications*. New York, NY, USA: Cambridge University Press, 2005.

[33] J. Kimionis, "Bistatic scatter radio for increased-range environmental sensing," Master's thesis, Technical University of Crete, Aug. 2013, supervisor A. Bletsas.

[34] E. Kampianakis, "Scatter radio sensor network with analog frequency modulation principles," Master's thesis, Technical University of Crete, Jul. 2014, supervisor A. Bletsas.

[35] F. W. J. Olver, D. W. Lozier, R. F. Boisvert, and C. W. Clark, *NIST handbook of mathematical functions*. New York, NY: Cambridge Univ. Press, 2010.

[36] P. N. Alevizos, Y. Fountzoulas, G. N. Karystinos, and A. Bletsas, "Log-linear-complexity GLRT-optimal noncoherent sequence detection for orthogonal and RFID-oriented modulations," *IEEE Trans. Commun.*, vol. 64, no. 4, pp. 1600–1612, Apr. 2016.

[37] P. N. Alevizos, "Channel coding and detection for increased range bistatic scatter radio," Master's thesis, Technical University of Crete, Oct. 2014, supervisor A. Bletsas.

[38] E. Biglieri, *Coding for Wireless Channels*. Springer, 2006.

[39] J. G. Proakis and M. Salehi, *Digital Communications*, 5th ed. New York, NY: McGraw-Hill, 2007.

[40] D. J. Costello and G. D. Forney Jr., "Channel coding: The road to channel capacity," *Proc. IEEE*, vol. 95, no. 6, pp. 1150–1177, Jun. 2007.

[41] S. M. Kay, *Fundamentals of statistical signal processing. [Volume I]. , Estimation theory*. Upper Saddle River (N.J.): Prentice Hall, 1993.

[42] B. C. Levy, *Principles of Signal Detection and Parameter Estimation*. New York: Springer, 2008.

[43] I. S. Gradshteyn and I. M. Ryzhik, *Table of Integrals, Series, and Products*. 7th ed. Elsevier/Academic Press, Amsterdam, 2007.